Published for SISSA by Springer

Received: July 9, 2025
Revised: September 24, 2025
Accepted: November 12, 2025
Published: January 5, 2026

Constraining four-heavy-quark operators with top-quark, Higgs, and electroweak precision data

Stefano Di Noi,[a] **Hesham El Faham**,[b] **Ramona Gröber**,[c] **Marco Vitti**[d,e] **and Eleni Vryonidou**[b]

[a] *Institute for Theoretical Physics, Karlsruhe Institute of Technology (KIT), Wolfgang-Gaede Straße 1, Karlsruhe D-76131, Germany*
[b] *Department of Physics and Astronomy, University of Manchester, Oxford Road, Manchester M13 9PL, U.K.*
[c] *Dipartimento di Fisica e Astronomia "G. Galilei", Università di Padova, and Istituto Nazionale di Fisica Nucleare, Sezione di Padova, Via Marzolo 8, I-35131 Padova, Italy*
[d] *Institute for Theoretical Particle Physics, Karlsruhe Institute of Technology (KIT), Wolfgang-Gaede Straße 1, Karlsruhe D-76131, Germany*
[e] *Institute for Astroparticle Physics, Karlsruhe Institute of Technology (KIT), Hermann-von-Helmholtz-Platz 1 Eggenstein-Leopoldshafen, Karlsruhe D-76344, Germany*

E-mail: stefano.dinoi@kit.edu, hesham.elfaham@manchester.ac.uk, ramona.groeber@pd.infn.it, marco.vitti@kit.edu, eleni.vryonidou@manchester.ac.uk

Abstract: We establish constraints on the dimension-six four-heavy-quark operators in the Standard Model Effective Field Theory (SMEFT) by synthesising LHC measurements of top-quark and single-Higgs production with electroweak precision observables. We scrutinise the choice of the γ_5 scheme in single-Higgs calculations, demonstrating its non-negligible impact on SMEFT fits.

Keywords: Electroweak Precision Physics, SMEFT

ArXiv ePrint: 2507.01137

https://doi.org/10.1007/JHEP01(2026)025

JHEP01(2026)025

Contents

1 Introduction

The absence of direct evidence for new light particles beyond the Standard Model (SM) at the Large Hadron Collider (LHC) has motivated a campaign of indirect searches in the SM Effective Field Theory (SMEFT) framework. In SMEFT, new-physics effects are parametrised through a series of higher-dimensional operators modifying the interactions of the SM particles. Thus, SMEFT provides a systematic and model-agnostic way of probing new physics in the absence of new light states. A key strength of the SMEFT framework lies in its ability to correlate effects across different sectors of the SM interactions. In order to fully exploit its potential in identifying signatures of physics beyond the SM, global analyses and interpretations within the SMEFT paradigm have become essential, prompting significant ongoing efforts [1–8].

JHEP01(2026)025

Such global interpretations are crucial, as they can reveal potential signs of new physics or, at the very least, place constraints on the energy scale at which new physics could appear by setting bounds on the Wilson Coefficients (WCs) of higher-dimensional operators. Additionally, global interpretations help identify sectors with greater potential for deviations from the SM by highlighting the least constrained operator classes. Notably, operators involving four heavy-quark fields stand out as among the least constrained by current experimental data. These induce contact interactions of four top quarks ($t\bar{t}t\bar{t}$), four bottom quarks ($b\bar{b}b\bar{b}$), and interactions involving a top-quark pair with a bottom-quark pair ($t\bar{t}b\bar{b}$).

Results from global fits indicate that the new-physics scale associated with this class of operators can be as low as a few hundred GeV; see, for example, the recent global analysis by the SMEFiT collaboration [5]. These loose constraints arise because, at tree level, these interactions are predominantly probed by $t\bar{t}t\bar{t}$ or $t\bar{t}b\bar{b}$ production, which suffer from large experimental uncertainties [9–11]. Moreover, these inclusive measurements are not sufficient to distinguish different colour and chirality structures in contact interactions, leading to flat directions that weaken the constraints.

These findings-together with model-building arguments suggesting that new physics might be top-philic [12–17]–have motivated indirect probes of the four-heavy contact operators via their higher-loop contributions to observables that are measured more precisely than multi-top-quark production. In particular, the effects of four-heavy-quark operators on electroweak precision observables (EWPO) [18–20], single-Higgs production in gluon fusion [21, 22], top-quark-pair production [23, 24] and flavour observables [20, 25] have been computed. These studies demonstrate that such indirect probes supply information complementary to four-top-quark production and must be included to obtain tighter limits on the strength of these interactions.

In this work we carry out a fit that combines direct and indirect probes, thereby exploiting their complementarity. Specifically, we include leading-order (LO) contributions to $t\bar{t}t\bar{t}$ and $t\bar{t}b\bar{b}$ production; next-to-leading-order (NLO) contributions to $t\bar{t}$ and $t\bar{t}H$ production; two-loop effects in gluon-fusion Higgs production ($gg \to H$) and Higgs decays, together with the two-loop contributions to EWPO.

The chiral nature of the four-fermion contact interactions in the SMEFT demands particular care in loop computations, because the Dirac algebra necessarily involves γ_5. Since γ_5 is intrinsically four-dimensional, one must define a consistent continuation to $d = 4 - 2\epsilon$ dimensions. In this work, we adopt two distinct continuation schemes: the *naïve dimensional regularisation* (NDR) scheme [26] and the *Breitenlohner-Maison-'t Hooft-Veltman* (BMHV) scheme [27, 28].

Provided that each scheme is implemented consistently, any differences in EFT matrix elements can be traced either to the scheme-dependent definition of the WCs [22] or to finite terms specific to the chosen renormalisation prescription [29]. This is due to the fact that NDR and BMHV predictions can be different in loop computations. We demonstrate this explicitly for the two-loop process of single-Higgs production and decay mediated by four-heavy-quark operators: in a dedicated fit, the bounds extracted for the WCs differ between the NDR and BMHV schemes. Such scheme dependence has been studied also in the context of di-Higgs production at the LHC [30], flavour physics [31–35]. It is worth noting

JHEP01(2026)025

that the choice of the γ_5 continuation scheme is not the only source of scheme dependence in loop computations [36–38].

The paper is organised as follows: in section 2, we state our flavour assumptions, introduce the SMEFT operators relevant to this study, and outline the computational setup. Section 3 presents our predictions for the processes under consideration and summarises the analytic expressions for the four-top-quark operators that modify the ggH and $\gamma\gamma H$ couplings in both the NDR and BMHV γ_5 schemes. The scheme dependence of the resulting bounds on the WCs is examined in section 4. Our fitting method and core results are detailed in section 5. Finally, section 6 summarises our findings.

2 Theoretical framework and computation setup

In this section, we discuss the SMEFT theoretical employed, along with the technical details underlying our computations.

2.1 SMEFT framework

A generic SMEFT Lagrangian, including terms up to $\mathcal{O}(\Lambda^{-4})$, can be written as

$$\mathcal{L}_{\text{SMEFT}} = \mathcal{L}_{\text{SM}} + \sum_i \frac{c_i^{(6)}\,\mathcal{O}_i^{(6)}}{\Lambda^2} + \sum_j \frac{c_j^{(8)}\,\mathcal{O}_j^{(8)}}{\Lambda^4} + \mathcal{O}(\Lambda^{-6})\,, \tag{2.1}$$

where $c_i^{(D)}$ and $\mathcal{O}_i^{(D)}$ are the WCs and SMEFT operators of mass dimension D, respectively, and Λ denotes the scale of new physics. Restricting to the dimension-six operators, the SMEFT prediction for cross section can be parametrised as

$$\sigma_{\text{SMEFT}} = \sigma_{\text{SM}} + \sigma_{\text{int}}^{(i)}\,\frac{c_i}{\Lambda^2} + \sigma_{\text{quad}}^{(i)}\,\frac{c_i^2}{\Lambda^4} + \sigma_{\text{cross}}^{(i,j)}\,\frac{c_i\,c_j}{\Lambda^4}\,. \tag{2.2}$$

Here σ_{int} originates from the interference between the SM and dimension-six SMEFT amplitudes scaling as Λ^{-2}, while σ_{quad} and σ_{cross} denote the diagonal (c_i^2) and off-diagonal ($c_i c_j$) quadratic contributions scaling as Λ^{-4}. An analogous parametrisation will be adopted for the partial widths, Γ. In all our results we set $\Lambda = 1\,\text{TeV}$.

We use a specific flavour assumption of the SMEFT focused on top-quark interactions:

$$\text{U}(3)_l \times \text{U}(3)_e \times \text{U}(2)_q \times \text{U}(2)_u \times \text{U}(3)_d \equiv \text{U}(2)^2 \times \text{U}(3)^3, \tag{2.3}$$

where the subscripts denote the five-fermion representations of the SM. This minimal relaxation of the $\text{U}(3)^5$ group allows for top-quark-chirality-flipping interactions, such as dipole interactions and modifications to the top-Yukawa coupling. In the widely-used Warsaw basis [39], the four-heavy subclass of dimension-six four-fermion operators are defined as follows:

$$\begin{aligned}
\mathcal{Q}_{qq}^{1(ijkl)} &= (\bar{q}_i\gamma^\mu q_j)(\bar{q}_k\gamma_\mu q_l), \quad & \mathcal{Q}_{qq}^{3(ijkl)} &= (\bar{q}_i\gamma^\mu \tau^I q_j)(\bar{q}_k\gamma_\mu \tau^I q_l),\\
\mathcal{Q}_{qu}^{1(ijkl)} &= (\bar{q}_i\gamma^\mu q_j)(\bar{u}_k\gamma_\mu u_l), \quad & \mathcal{Q}_{qu}^{8(ijkl)} &= (\bar{q}_i\gamma^\mu T^A q_j)(\bar{u}_k\gamma_\mu T^A u_l),\\
& & \mathcal{Q}_{uu}^{(ijkl)} &= (\bar{u}_i\gamma^\mu u_j)(\bar{u}_k\gamma_\mu u_l),
\end{aligned}$$

JHEP01(2026)025

where only third-generation quark fields are understood and we have used the notation $\mathcal{Q}$ to denote operators written in said Warsaw basis, with the corresponding WCs denoted as C_i. However, in this work, we use operators aligned with the `dim6top` [40] and `SMEFTatNLO` [23] conventions, hereafter referred to as the 'top basis' — in which the operators are written as $\mathcal{O}_i$ with Wilson coefficients c_i. The translations of four-heavy coefficients at tree level from the Warsaw basis to the top basis are as follows:

$$\begin{aligned} c^1_{QQ} &= 2C^{(1)}_{qq} - \frac{2}{3}C^{(3)}_{qq}, & c^1_{Qt} &= C^{(1)}_{qu}, \\ c^1_{tt} &= C^{(1)}_{uu}, & c^8_{QQ} &= 8C^{(3)}_{qq}, \\ c^8_{Qt} &= C^{(8)}_{qu}. \end{aligned} \tag{2.4}$$

The corresponding state-of-the-art constraints are reported in the recent global fit of ref. [5]. We note here that, in all our computations, we adopt the definition of the four-heavy operator, $\mathcal{O}^8_{QQ}$, in terms of Warsaw-basis operators, i.e. $\mathcal{O}^8_{QQ} = \mathcal{Q}^{(3)}_{qq}/8 + \mathcal{Q}^{(1)}_{qq}/24$, rather than $\mathcal{O}^8_{QQ} = \frac{1}{2}(\bar{Q}\gamma^\mu T^A Q)(\bar{Q}\gamma_\mu T^A Q)$. The two expressions differ by an evanescent operator, as also discussed in ref. [20]. Numerical results can differ between the two definitions when the evanescent operator contributes. All our results are consistent with the former definition, and we will comment on this further.

2.2 Computation setup

For all our predictions, we utilise `MadGraph5_aMC@NLO` [41] and the `SMEFT@NLO` [23] package, with the exceptions being $gg \to H$, for which we employ the analytic expression given in ref. [22] and the EWPO, for which we use the expressions in eq. (3.1) extracted from [19, 20] — see dedicated discussions below. The parton distribution functions (PDF) set `NNPDF3.1` in the five-flavour scheme at NLO with $\alpha_s(m_Z) = 0.118$ [42] is used as input for all Monte Carlo (MC) simulations through the `LHAPDF` interface [43]. All computations are carried out in the G_F scheme [44, 45], which is recommended for SMEFT analyses by the LHC EFT WG [46]. The Fermi constant value is set to $G_F = 1.16637 \times 10^{-5}\,\text{GeV}^{-2}$. The masses of the Higgs boson and the top quark are set to $m_H = 125\,\text{GeV}$ and $m_t = 172\,\text{GeV}$, respectively.

As will be relevant later, it is important to note that in `SMEFT@NLO` [23], in $d \neq 4$ dimensions, γ_5 is treated as anti-commuting, and the cyclic property of Dirac matrices traces is not maintained following the KKS scheme [47]. The latter is understood to be equivalent to the NDR scheme supplemented with a fixed reading point.

The factorisation and renormalisation scales, μ_F and μ_R, are set to half of the sum of the masses of the final state particles. The scale μ_{EFT} introduced in the counterterms of the WCs is set to μ_R to ensure $\overline{\text{MS}}$ renormalisation for the EFT poles [24]. The effects of renormalisation group equations (RGEs) on the WCs are not considered in this work, and we interpret the WCs at a typical electroweak (EW) scale. We refer to refs. [48–51] for RGE effects in this context. Considering the EWPO at scale $Q \sim m_Z$ and four-top-quark production at $Q \sim 2m_t$, we adopt scales within a factor of four of each other and thus expect RGE effects to be under control.

JHEP01(2026)025

3 Studied processes

In this section, we review the characteristic features of the LHC processes analysed in this work: four-top-quark production; top-quark pair production; top-quark pair production in association with a Higgs boson; single-Higgs production with its subsequent decay. Finally, we discuss the EWPO predictions employed in our analysis.

We keep our discussion of top-quark processes concise, since these computations are already well established and extensively discussed in the literature. For the EWPO predictions, however, we explicitly report the individual contributions to each of the WCs, as we are not aware of any previous work where this has been done. In section C, we provide the details of how these contributions were extracted using the EWPO two-loop results of ref. [20]. Finally, our treatment of single-Higgs production is comparatively more extensive, as we use it to illustrate the emergence of the γ_5-scheme dependence in the computation — an aspect that is central to the discussion in the following section. All results discussed in this section are presented in the NDR scheme, unless explicitly stated otherwise, as in the context of single-Higgs production.

3.1 Four-top-quark production

Our $pp \to t\bar{t}t\bar{t}$ predictions are listed in table 3 of section B. As demonstrated in ref. [52], subleading terms stemming from the interference of four-fermion operators with weakly mediated SM amplitudes play a non-negligible role; all such contributions are therefore included in our calculation. It is worth noting that, unlike $t\bar{t}$ production, the richer colour structure of the $pp \to t\bar{t}t\bar{t}$ process allows colour-singlet operators to interfere with the QCD SM amplitudes already at LO.

In the pure SM, subleading EW contributions almost exactly cancel among themselves [53] making the leading NLO QCD prediction highly reliable. In the EFT, however, such cancellation is not guaranteed because the SMEFT operators alter the kinematic structure of the amplitudes. A fully consistent NLO prediction in the SMEFT would thus require the complete set of NLO QCD *and* EW corrections — an undertaking that is presently beyond the reach of existing automated tools. Therefore, we employ only tree-level predictions for this process.

3.2 Top-quark pair production (and in association with a Higgs)

In $pp \to t\bar{t}(H)$, four-fermion operators that involve a third-generation doublet contribute at tree level through b-quark-initiated amplitudes. The interference of colour-singlet four-fermion operators with the SM vanishes at tree level when only purely QCD-induced amplitudes are considered [54], because the top quarks are always produced in a colour-octet configuration.[1] At NLO in QCD, however, both real and virtual corrections alter the colour flow and can induce a non-zero interference for colour-singlets.

Inclusive predictions for all processes as well as the differential predictions in the Higgs boson transverse momenta, p_T^H, for both the SM and the SMEFT are collected in tables 2

[1] For weak-mediated Born amplitudes, i.e. $t\bar{t}$ production via an s-channel weak boson, colour-singlets can already interfere at LO. These contributions are generally expected to be subdominant and are not considered here.

JHEP01(2026)025

and 3 of section B.[2] The SMEFT results are separated into linear, $\mathcal{O}(\Lambda^{-2})$, and (off-) diagonal quadratic, $\mathcal{O}(\Lambda^{-4})$, terms. As previously mentioned, at LO, the operators under study contribute only through b-quark-initiated channels so the diagonal-quadratic piece from c^1_{tt} vanishes. Because c^1_{tt} first appears at one loop, obtaining its quadratic contribution would require squaring the loop amplitudes rendering it beyond the perturbative order considered in this work.

We observe that c^1_{Qt} dominates the SMEFT corrections at NLO, providing by far the largest linear contribution to the cross section. This is the case in both $t\bar{t}$ and $t\bar{t}H$ production. The dominance of this contribution can be traced back to cancellations among different partonic channels and phase-space regions for all coefficients except c^1_{Qt} [23]. Moreover, the contribution of the right-handed four-top-quark operator, $\mathcal{O}^1_{tt}$, features some strong cancellation between the gluon- and quark-initiated channels in $t\bar{t}H$ production. This cancellation amplifies the scale dependence and results in sizeable QCD uncertainties for the linear contribution, as illustrated in table 3. The same pattern is visible differentially in one of the p_T^H bins in table 2. In $t\bar{t}$ production, this effect is absent in the inclusive rate. Moving to the off-diagonal quadratic terms, at LO, interference between colour-singlet and colour-octet structures — whether between SM and EFT amplitudes or between two different EFT operators — vanishes exactly, and so only singlet-singlet and octet-octet combinations survive, as shown in table 3. At NLO, real emissions or virtual gluon exchange can mix the colour flows, generating singlet-octet cross terms which are numerically tiny-cross terms consistent with zero at the 2σ level are therefore omitted from the tables for clarity.

Finally, in figure 1, the differential distributions of the top-quark-pair invariant mass, $m_{t\bar{t}}$, and the Higgs transverse momentum, p_T^H, are displayed in the left and right panels, respectively. For $\mathcal{O}(1)$ WCs, the four-heavy operators modify the SM prediction by at most the percent level. This mild impact is expected, given both the one-loop suppression and the small b-quark parton density driving these contributions. The dominant correction comes from $\mathcal{O}^1_{Qt}$: its contribution is significant in the low-invariant-mass region of the $t\bar{t}$ spectrum while it induces an essentially flat shift in the p_T^H distribution. All other operators yield sub-percent effects; in some kinematic bins their contributions even change sign, as indicated by the dashed curves in the figures.

3.3 Electroweak precision observables

Our EWPO predictions are obtained at the two-loop level leveraging the work of ref. [20] and reported here in eq. (3.1). These results are quoted in the NDR scheme. It is also important to emphasise that all EWPO results were extracted in the original Warsaw basis from ref. [20]. These results are expected to be consistent with our `SMEFT@NLO` calculations. Although the latter employs the rotations defined in eq. (2.4), it ultimately remains formulated in the Warsaw basis. In summary, extracting the EWPO results directly in either the original Warsaw basis or the top basis is not expected to affect the WCs contributions, with the sole exception of the four-heavy colour-octet operator. The original Warsaw basis choice for said operator will differ by an evanescent contribution compared to its contribution

[2] Differential predictions in the top-quark-pair invariant mass, $m_{t\bar{t}}$, for $t\bar{t}$ production are omitted here for brevity, but can be provided upon request.

JHEP01(2026)025

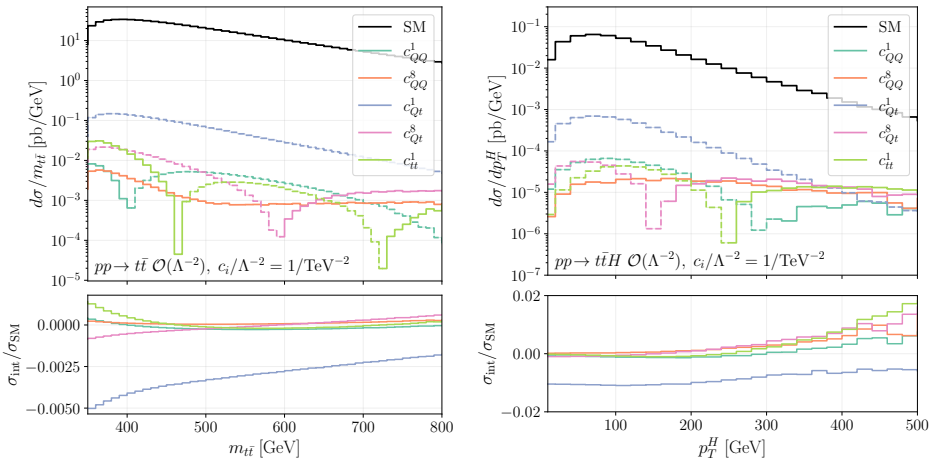

Figure 1. Differential distributions of the top-quark-pair invariant mass in $t\bar{t}$ (left) and of the Higgs transverse momentum in $t\bar{t}H$ (right). The curves show the linear SMEFT contributions of the five four-heavy operators, compared to the NLO SM prediction. The absolute values are plotted, and the dashed lines indicate where the interference becomes destructive — that is, where the contributions are negative.

defined with two colour-octet currents-see discussion below eq. (2.4). The reason is due to the mapping in section 2.1 being a tree-level one (cf. ref. [20]). We further note that this evanescent term can be numerically significant, and a substantial shift in the corresponding contribution would be expected had the results in the top basis conventions of ref. [20] been employed from the outset.

$$
\begin{aligned}
\delta\Gamma_Z^{b\bar{b}} &= 9.5412\times10^{-4}\,c^1_{QQ} + 1.0098\times10^{-4}\,c^8_{QQ} - 1.1409\times10^{-3}\,c^1_{Qt} \\
&\quad + 4.4956\times10^{-7}\,c^8_{Qt} - 3.12\times10^{-6}\,c^1_{tt}, \\
\delta R_c &= -9.699\times10^{-5}\,c^1_{QQ} - 1.0265\times10^{-5}\,c^8_{QQ} + 1.1598\times10^{-4}\,c^1_{Qt} \\
&\quad - 4.5701\times10^{-8}\,c^8_{Qt} + 3.1718\times10^{-7}\,c^1_{tt}, \\
\delta R_l &= 1.1688\times10^{-2}\,c^1_{QQ} + 1.2371\times10^{-3}\,c^8_{QQ} - 1.3977\times10^{-2}\,c^1_{Qt} \\
&\quad + 5.5074\times10^{-6}\,c^8_{Qt} - 3.8222\times10^{-5}\,c^1_{tt}, \\
\delta R_b &= 4.4158\times10^{-4}\,c^1_{QQ} + 4.6736\times10^{-5}\,c^8_{QQ} - 5.2803\times10^{-4}\,c^1_{Qt} \\
&\quad + 2.0806\times10^{-7}\,c^8_{Qt} - 1.444\times10^{-6}\,c^1_{tt}, \\
\delta A_b &= 2.4597\times10^{-4}\,c^1_{QQ} + 3.2227\times10^{-5}\,c^8_{QQ} - 2.9442\times10^{-4}\,c^1_{Qt} \\
&\quad + 5.834\times10^{-7}\,c^8_{Qt} + 5.7326\times10^{-5}\,c^1_{tt}, \\
\delta A_{b,\text{FB}} &= 2.5306\times10^{-4}\,c^1_{QQ} + 8.3078\times10^{-5}\,c^8_{QQ} - 3.0434\times10^{-4}\,c^1_{Qt} \\
&\quad + 5.3495\times10^{-6}\,c^8_{Qt} + 5.2565\times10^{-4}\,c^1_{tt}\,.
\end{aligned}
\tag{3.1}
$$

The definitions of the observables, as well as details of the computation and numerical inputs, are provided in section C. We note that (off-)diagonal quadratic EFT contributions are strongly suppressed relative to the linear contributions shown in eq. (3.1). Moreover,

JHEP01(2026)025

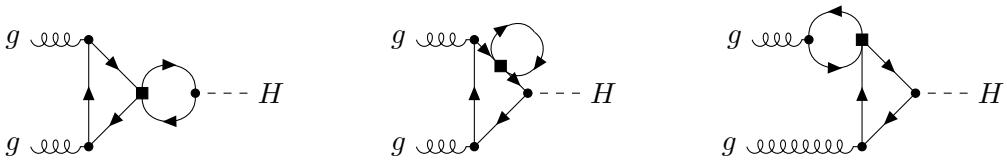

(a) Higgs-top-quark coupling. (b) Top-quark propagator. (c) Gluon-top-quark vertex.

Figure 2. Feynman diagrams illustrating the corrections to $gg \to H$ induced by four-top-quark SMEFT operator insertions.

the contributions of c_{Qt}^8 and c_{tt}^1 are purely two-loop induced, as they do not contribute to the EWPO at one loop.

Although the one-loop contributions are not shown here-see section C for said contributions-in comparison, we find the two-loop corrections to be negligible for all observables except for the bottom-quark asymmetry, A_b, and its forward-backward counterpart, $A_{b,\mathrm{FB}}$, where they are significant.

3.4 Single-Higgs production in gluon-fusion and Higgs decays

Higgs production via gluon fusion and its decays into gluons and photons are loop-induced already at LO. Four-top-quark operators contribute for the first time through two-loop diagrams, such as those shown in figure 2 for the production process.

For single-Higgs production, we adopt the results of ref. [22]. A key challenge in these computations arise from the presence of γ_5 in the loop amplitudes rendering a delicate treatment necessary when dimensional regularisation is used. It has been shown in ref. [22] that isolated contributions of four-top-quark operators depend on the continuation scheme of the γ_5 matrix to $d = 4 - 2\epsilon$ dimensions. The reference studied two schemes: the NDR [26] and the BMHV scheme [27, 28]. Whilst the former is algebraically inconsistent in the presence of traces involving six or more γ^μ matrices [47, 55–57], the latter remains consistent but the regulator spuriously breaks chiral symmetries and hence requires symmetry-restoring counterterms [58–64].

The continuation-scheme dependence is expected to cancel upon matching, once a process-specific set of operators at a given loop order is included.[3] We adopt the loop-order definitions of refs. [65, 66], which requires the assumption of weakly interacting and renormalisable UV models. Scheme-independent results can be achieved by including operators that enter at a lower loop order. In section A, we specify those additional operators for the case of ggH and $\gamma\gamma H$ and we provide results for the complete contribution to the renormalised matrix element, together with auxiliary quantities not defined in this section. Since the focus of the present paper is on the four-top operators, in this section we only show the contribution of the latter to the renormalised matrix element, which we denote as $\mathcal{M}_{\mathrm{OS}}^{ggH,4\mathrm{t}}$ and it reads as follows:

$$\mathcal{M}_{\mathrm{OS}}^{ggH,4\mathrm{t}} = \left(c_{Qt}^1 + \left(c_F - \frac{c_A}{2}\right) c_{Qt}^8\right) \mathcal{K}_{tG} \frac{1}{\Lambda^2} \mathcal{M}_{tG}^{ggH} + \left(c_{Qt}^1 + c_F c_{Qt}^8\right) \frac{1}{\Lambda^2} \left(B_{ggH} + \mathcal{K}_{t\varphi}\right) \mathcal{M}_{\mathrm{SM}}^{ggH}, \tag{3.2}$$

[3] This applies to scenarios in which UV divergences are absent in the UV model, a feature that is guaranteed for the operators considered here by the superficial degree of divergence [29].

JHEP01(2026)025

$$\mathcal{K}_{tG}=\begin{cases}\frac{\sqrt{2}m_t g_s}{16\pi^2 v} & \text{(NDR)}\\ 0 & \text{(BMHV)},\end{cases}\qquad \mathcal{K}_{t\varphi}=\begin{cases}\frac{m_H^2-4m_t^2}{16\pi^2} & \text{(NDR)}\\ 0 & \text{(BMHV)},\end{cases} \tag{3.3}$$

$$B_{ggH}=\frac{4m_t^2-m_H^2}{8\pi^2}\left(\beta\log\left(\frac{\beta-1}{\beta+1}\right)+2+\log\left(\frac{\mu_R^2}{m_t^2}\right)\right),\quad \beta=\sqrt{1-\frac{4m_t^2}{m_H^2}}. \tag{3.4}$$

The matrix element in eq. (3.2) has been obtained in the on-shell (OS) renormalisation scheme for the top-quark mass, whilst the operators are renormalised in the $\overline{\text{MS}}$ scheme. We note that this differs from the renormalisation scheme of ref. [22]. The scheme dependence in eq. (3.2) and in the following eq. (3.5) is parametrised by the $\mathcal{K}$ terms in eq. (3.3). The scheme dependence arises, in principle, from all the diagrams sketched in figure 2. In particular, the diagram topology in figure 2(a) gives the scheme-dependent contribution associated to $\mathcal{K}_{t\varphi}$, the diagram topology in figure 2(b) is nullified by the on-shell top mass counterterm and the diagram topology in figure 2(c) gives the scheme-dependent contribution associated to $\mathcal{K}_{tG}$. A detailed diagram-by-diagram analysis can be found in ref. [22], to which we refer the interested reader.

Finally, we note that only the two operators $\mathcal{O}_{Qt}^1$ and $\mathcal{O}_{Qt}^8$ contribute to the matrix element in eq. (3.2). This is a consequence of the colour structure of the diagrams and the on-shell kinematic configurations of the external states.

The matrix element for the Higgs-photon coupling ($\gamma\gamma H$) can be obtained by performing the replacements indicated in section A on eq. (3.2) yielding

$$\mathcal{M}_{\text{OS}}^{\gamma\gamma H,4\text{t}}=\left(c_{Qt}^1+c_F c_{Qt}^8\right)\mathcal{K}_{tG}\frac{Q_t e}{g_s}\frac{1}{\Lambda^2}\mathcal{M}_{t\gamma}^{\gamma\gamma H}+\left(c_{Qt}^1+c_F c_{Qt}^8\right)\frac{1}{\Lambda^2}(B_{ggH}+\mathcal{K}_{t\varphi})\mathcal{M}_{\text{SM}}^{\gamma\gamma H}. \tag{3.5}$$

We note that different combination of WCs enter in eq. (3.2) compared to eq. (3.5)–first term of the former. The phenomenological consequences of this observation are discussed in the following section.

4 Interpretation of SMEFT constraints in different γ_5 schemes

In this section, we perform a simplified (toy) fit to assess the impact of the γ_5 prescription on the bounds on WCs from single-Higgs production. This fit uses the Higgs signal strength and its associated data from ref. [67]. We restrict our study to the dominant gluon-fusion channel and consider only total production rates, since measurements of the Higgs transverse-momentum spectrum are not yet available. We use the same numerical inputs as in section 2.2 and we set $\mu_R=\mu_F=m_H/2$ for Higgs production and $\mu_R=m_H$ for the partial widths [68].

In table 4 of section B we list the numerical results for the single-Higgs production cross section, σ, and the Higgs partial width, Γ, computed in both γ_5 schemes using the formulae derived in the previous section. We omit the $\mathcal{O}(\Lambda^{-4})$ terms, as they enter at one loop order higher than the SM-$\mathcal{O}(\Lambda^{-2})$ interference.

The theoretical signal strengths, μ^{Th}, used in the fit are defined as follows:

$$\mu_X^{\text{Th}}=\frac{\sigma_{\text{SMEFT}}\text{BR}(H\to X)_{\text{SMEFT}}}{\sigma_{\text{SM}}\text{BR}(H\to X)_{\text{SM}}},\qquad X\equiv[\gamma\gamma,W^+W^-,ZZ,b\bar{b},\tau^+\tau^-,\mu^+\mu^-]. \tag{4.1}$$

In eq. (4.1), the same K-factor is used to account for higher-order corrections both in the SM and linear, $\mathcal{O}\left(\Lambda^{-2}\right)$, EFT contributions to the production cross section and so it cancels out in the signal strengths.

JHEP01(2026)025

Concerning the branching ratios, $\mathrm{BR}(H \to X)$, in eq. (4.1), four-top-quark operators modify only the loop-induced partial widths $H \to gg$ and $H \to \gamma\gamma$-later denoted as Γ_{gg} and $\Gamma_{\gamma\gamma}$, respectively. Consequently the total Higgs width, Γ^{Tot}, changes and it multiplies all branching ratios by a common factor. Every theoretical signal strength in our fit therefore receives this universal rescaling — except for $\mu^{\mathrm{Th}}_{\gamma\gamma}$. Said channel is additionally affected by the process-specific four-top-quark contribution given in eq. (3.5). In particular, we have

$$\Gamma^{\mathrm{Tot}} = \Gamma^{\mathrm{Tot}}_{\mathrm{SM}} + K_{gg}\Gamma^{gg}_{\mathrm{int}} + K_{\gamma\gamma}\Gamma^{\gamma\gamma}_{\mathrm{int}}, \tag{4.2}$$

where $\Gamma^{gg}_{\mathrm{int}}$ and $\Gamma^{\gamma\gamma}_{\mathrm{int}}$ can be read from table 4, whilst the K-factors K_{gg} and $K_{\gamma\gamma}$ are obtained as the ratio between the SM best estimates [69–82] and the SM values in table 4. The following are the values we employ [68]: $\Gamma^{\mathrm{Tot}}_{\mathrm{SM}} = 4.088\,\mathrm{MeV}$, $K_{gg} = 1.707$, $K_{\gamma\gamma} = 0.913$.

We present here the theoretical signal strengths, expanded to linear order in the WCs, in the NDR scheme:

$$\begin{aligned}
\mu^{\mathrm{Th}}_{\gamma\gamma} &= 1 - 0.0159 \times c^1_{Qt} - 0.00239 \times c^8_{Qt} \\
&\quad - 6.60 \times 10^{-5}(c^1_{Qt})^2 - 2.34 \times 10^{-5}(c^8_{Qt})^2 - 9.34 \times 10^{-5} c^1_{Qt} c^8_{Qt}, \\
\mu^{\mathrm{Th}}_{\mathrm{Y}} &= 1 - 0.0186 \times c^1_{Qt} - 0.00606 \times c^8_{Qt} \\
&\quad - 1.47 \times 10^{-5}(c^1_{Qt})^2 - 1.17 \times 10^{-6}(c^8_{Qt})^2 - 8.39 \times 10^{-6} c^1_{Qt} c^8_{Qt},
\end{aligned} \tag{4.3}$$

and the BMHV one:

$$\begin{aligned}
\mu^{\mathrm{Th}}_{\gamma\gamma} &= 1 - 0.00451 \times c^1_{Qt} - 0.00601 \times c^8_{Qt} \\
&\quad - 2.53 \times 10^{-6}(c^1_{Qt})^2 - 4.50 \times 10^{-6}(c^8_{Qt})^2 - 6.75 \times 10^{-6} c^1_{Qt} c^8_{Qt}, \\
\mu^{\mathrm{Th}}_{\mathrm{Y}} &= 1 - 0.00491 \times c^1_{Qt} - 0.00655 \times c^8_{Qt} \\
&\quad - 5.66 \times 10^{-7}(c^1_{Qt})^2 - 1.01 \times 10^{-6}(c^8_{Qt})^2 - 1.51 \times 10^{-6} c^1_{Qt} c^8_{Qt},
\end{aligned} \tag{4.4}$$

where $\mathrm{Y} \equiv [\ W^+W^-,\ ZZ,\ b\bar{b},\ \tau^+\tau^-,\ \mu^+\mu^-]$.

In figure 3 we display the two-dimensional $\Delta\chi^2$ contours for the single-Higgs production fit in the $(c^1_{Qt},\, c^8_{Qt})$ plane. This result highlights the scheme dependence introduced by the choice of γ_5-continuation prescription. The analysis is restricted to four-top-quark operators and the fit retains all linear, quadratic, and mixed (cross) terms in eqs. (4.3) and (4.4).

As can be inferred from figure 3, the fit can distinguish between c^1_{Qt} and c^8_{Qt} in NDR but finds a flat direction for $c^1_{Qt} + c_F c^8_{Qt}$ in BHMV. This can be understood by inspecting eq. (3.2): in the BMHV scheme, contributions of the type shown in figure 2(c) vanish, leaving a degeneracy in the WCs. Conversely, in the NDR scheme, they are non-vanishing and are proportional to the linear combination $c^1_{Qt} + \left(c_A - \frac{c_F}{2}\right) c^8_{Qt}$, which lifts the degeneracy.

As detailed in section A, the WCs of operators entering at one-loop order depend on the scheme in such a way that they compensate for the scheme-dependent four-top-quark contribution. This observation highlights that a γ_5-prescription-independent result can be obtained only when a sufficiently complete set of SMEFT operators is included, as demonstrated in ref. [22]. If those additional operators are omitted, our fit — restricted to four-quark operators — must be interpreted differently in the NDR and BMHV schemes. Indeed, since the four-top operators behave differently in the two schemes, the corresponding fits probe distinct UV scenarios: either those that generate only four-top-quark operators

JHEP01(2026)025

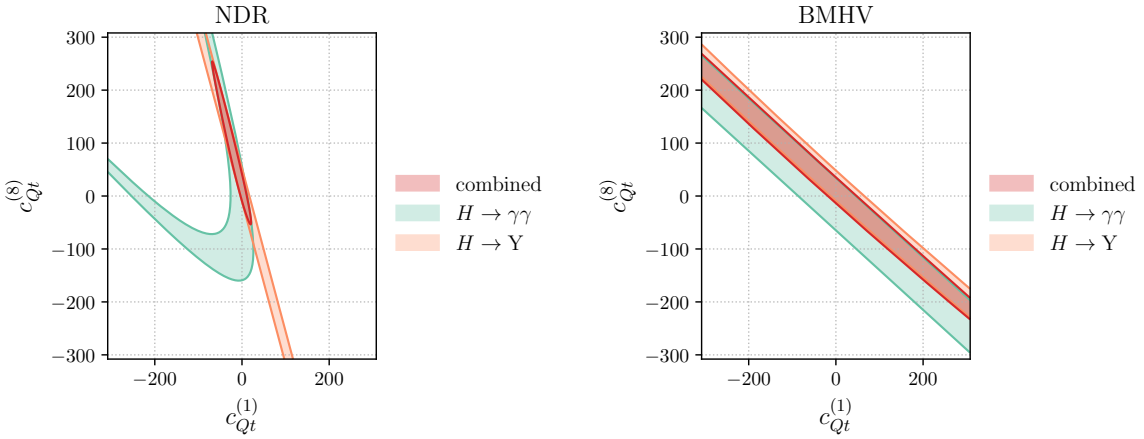

Figure 3. $\Delta\chi^2$ contours for the single-Higgs production fit in the (c_{Qt}^1, c_{Qt}^8) plane, shown for each decay channel, i.e. Y and $\gamma\gamma$ and for their combination, labelled as 'combined'. The left (right) panel corresponds to the NDR (BMHV) γ_5 scheme. A pronounced flat direction emerges in the BMHV fit, whereas no such degeneracy appears in the NDR scheme.

in the NDR scheme, or those that generate only four-top-quark operators in the BMHV scheme. These represent two separate classes of UV models.

5 Constraining four-quark operators: fit method, inputs and results

5.1 Fit method

We analyse the impact of SMEFT operators on measured inclusive and differential cross sections, σ_{Ex}, by performing individual and marginalised χ^2 fits. For an operator coefficient c_i, the theoretical cross section, σ_{Th}, in each bin, can be written as shown in eq. (2.2)

When statistical and systematic uncertainties are provided separately by the experimental collaborations, the total experimental uncertainty, Δ_{Ex}, in each bin is determined by combining both uncertainties in a quadrature, i.e. assuming no correlation-the total experimental uncertainty provided directly by the collaborations is used when available. The normalisation, Δ_{Tot}, entering the test statistic is the quadrature sum of experimental and theoretical uncertainties, the latter being the QCD scale uncertainties of SM predictions. Conservatively, we choose that as the maximum of the scale uncertainty envelope.

For each bin, the χ^2 contribution is therefore calculated as

$$\chi^2_{\mathrm{bin}} = \left(\frac{\sigma_{\mathrm{Ex}} - \sigma_{\mathrm{Th}}}{\Delta_{\mathrm{Tot}}}\right)^2, \tag{5.1}$$

and the total χ^2 is obtained by summing over all bins, as well as over all considered observables and processes:

$$\chi^2 = \sum_{\text{proc.}} \sum_{\text{obs.}} \sum_{\text{bins}} \chi^2_{\mathrm{bin}}. \tag{5.2}$$

Observables from different experiments are assumed to be uncorrelated. Finally, for the EWPO fit, we use the correlations between the different observables as quoted in ref. [83].

JHEP01(2026)025

Tag	$\sqrt{s}$, $\mathcal{L}$	Final state	Observable	$n_{\text{dat.}}$	Ref.(Ex)	Location/HEPData	Ref.(Th)
			$pp \to t\bar{t}$				
$\text{CMS}_{t\bar{t}}$	13 TeV, 137 fb^{-1}	lepton+jets	$d\sigma/dm_{t\bar{t}}$	15	[84]	/Table 37	[84]
$\text{ATLAS}_{t\bar{t}}$	13 TeV, 36 fb^{-1}	lepton+jets	$d\sigma/dm_{t\bar{t}}$	9	[85]	/Table 617	[85]
			$pp \to t\bar{t}H$				
$\text{ATLAS}_{t\bar{t}H}$	13 TeV, 140 fb^{-1}	$H \to b\bar{b}$	$d\sigma/dp_T^H$	6	[86]	Figure 3 in the ref./	[87]
			$pp \to t\bar{t}t\bar{t}$				
CMS_{4t}	13 TeV, 138 fb^{-1}	multi-leptons	$\sigma^{\text{tot.}}_{t\bar{t}t\bar{t}}$	1	[10]	/Figure 8	[88]
ATLAS_{4t}	13 TeV, 140 fb^{-1}	multi-leptons	$\sigma^{\text{tot.}}_{t\bar{t}t\bar{t}}$	1	[9]	/Table 17	[88]
			$gg \to H$				
CMS_{ggH}	13 TeV, 138 fb^{-1}	$W^+W^-, ZZ, b\bar{b}, \tau^+\tau^-, \mu^+\mu^-$	$\mu_{\text{Y}}^{\text{Ex}}$	1	[67]	/Table 12	eqs. (4.3) and (4.4)
CMS_{ggH}	13 TeV, 138 fb^{-1}	$\gamma\gamma$	$\mu_{\gamma\gamma}^{\text{Ex}}$	1	[67]	/Table 12	eqs. (4.3) and (4.4)
			$pp \to t\bar{t}b\bar{b}$				
$\text{ATLAS}_{t\bar{t}b\bar{b}}$	13 TeV, 36.1 fb^{-1}	lepton+jets	$\sigma^{\text{tot.}}_{t\bar{t}b\bar{b}}$	1	[89]	/Table 5	as in [5]
$\text{CMS}^1_{t\bar{t}b\bar{b}}$	13 TeV, 35.9 fb^{-1}	all-jets	$\sigma^{\text{tot.}}_{t\bar{t}b\bar{b}}$	1	[11]	Figure 3 in the ref./	as in [5]
$\text{CMS}^2_{t\bar{t}b\bar{b}}$	13 TeV, 35.9 fb^{-1}	dilepton	$\sigma^{\text{tot.}}_{t\bar{t}b\bar{b}}$	1	[90]	Table 4 in ref. (FPS)/	as in [5]
$\text{CMS}^3_{t\bar{t}b\bar{b}}$	13 TeV, 35.9, fb^{-1}	lepton+jets	$\sigma^{\text{tot.}}_{t\bar{t}b\bar{b}}$	1	[90]	Table 4 in ref. (FPS)/	as in [5]
			EWPO				
EWPO^1	Z-pole, /	Z decays	$\Gamma_Z^{b\bar{b}}, R_c, R_l, R_b$	1	[83]	Tables 7.1 and 8.4 in ref.	[91]
EWPO^2	Z-pole, /	Z decays	$A_b, A_{b,\text{FB}}$	1	[83]	Table 8.4 in ref.	[83]

Table 1. Summary of the inputs used in the fit. For each dataset we list, from left to right: (i) the dataset label; (ii) the centre-of-mass energy and integrated luminosity; (iii) the measured final state; (iv) the observable under study; (v) the number of data points; (vi) the experimental publication; (vii) the location of the experimental data (either in the publication or via its HEPData entry[4]); and (viii) the reference used for theoretical predictions.

5.2 Fit inputs

We discuss here the inputs for the processes included in our fit, which are summarised in table 1.

***pp* → *tt̄*.** The SM predictions in the bins of $\text{ATLAS}_{t\bar{t}}$ are taken from the corresponding publication [85], where MC simulations were generated using `Powheg-Box` v2 [92–95] interfaced with `Pythia` 8.210 [96]. The cross-section normalisation of these MC samples is set to the NNLO + next-to-next-to-leading-logarithmic (NNLL) QCD prediction [97–103], as indicated explicitly in table 1 of the publication. Predictions and measurements from $\text{ATLAS}_{t\bar{t}}$ are normalised to the total cross section of 832^{+20}_{-29} pb, as reported therein.

The SM predictions in the bins of $\text{CMS}_{t\bar{t}}$ are also taken from the corresponding publication [84]. The cross-section normalisation of these MC samples is set to the NNLO in the strong coupling constant including the resummation of NNLL soft-gluon terms calculated with TOP++ (version 2.0) [97]. This amounts to a normalisation factor, i.e. the inclusive $t\bar{t}$ production cross section, of 832^{+40}_{-46} pb. The SM theoretical uncertainties are taken from the respective publications.

***pp* → *tt̄H*.** We use the SM predictions and the associated uncertainties provided in the analysis of ref. [87]. We use the experimental data from the most recent measurement of ref. [86] reporting a measured total cross section of $411^{+24\%}_{-22\%}$ fb. The SM differential

[4] https://www.hepdata.net/

JHEP01(2026)025

predictions [68, 104–109] extracted from ref. [87] are in good agreement with our own results presented in table 2 of section B.

pp → ttttbar. For both datasets, we adopt the SM cross section of ref. [88], computed at NLO (QCD+EW)+NLL accuracy, yielding $13.37^{+7.77\%}_{-13.3\%}$ fb.

pp → ttbb. We extract the experimental measurements and theoretical predictions — for *both* the SM-assigned a 10% theoretical uncertainty- and the SMEFT — from ref. [5].[5]

gg → H. The analysis presented in ref. [67] reports signal-strength modifiers, $\mu_i^{\rm Ex}$, categorised through their decay modes i, with uncertainties representing the total experimental error, combining both systematic and statistical contributions. These results are summarised as follows:

$$\begin{aligned} \mu_{\mu\mu}^{\rm Ex} &= 0.33^{+0.74}_{-0.70}\,, \quad \mu_{\tau\tau}^{\rm Ex} = 0.66^{+0.21}_{-0.21}\,, \quad \mu_{ZZ}^{\rm Ex} = 0.93^{+0.14}_{-0.13}\,, \\ \mu_{WW}^{\rm Ex} &= 0.90^{+0.11}_{-0.10}\,, \quad \mu_{bb}^{\rm Ex} = 5.31^{+2.97}_{-2.54}\,, \quad \mu_{\gamma\gamma}^{\rm Ex} = 1.08^{+0.12}_{-0.11}\,. \end{aligned} \tag{5.3}$$

The results reported in eq. (5.3) are of the gluon-fusion production mode and constitute the experimental input for our fit. Given that gluon fusion is directly sensitive to the operators we consider and is the dominant production mode for single-Higgs production, we do not expect significant sensitivity from other production modes.We set the SM prediction to unity.

EWPO. Our predictions are obtained at the two-loop level leveraging the work of ref. [20] as discussed in section 3.3 and in section C. Experimental measurements and correlations are taken from ref. [83]. SM predictions for all observables apart from A_b and $A_{b,\rm FB}$ are extracted from table 2 of ref. [91]. SM predictions of A_b and $A_{b,\rm FB}$ are taken directly from table 8.4 in ref. [83].

5.3 Fit results

Figure 4 shows the two-dimensional $\Delta\chi^2$ contours at 95% CL for the case where only linear EFT terms are included whilst figure 5 corresponds to the scenario where quadratic contributions are also taken into account. In both panels, we display the contours for the combined fit (all processes) under two distinct scenarios: one in which only the two WCs of interest are varied (black solid-line contour, labelled as 'comb-2D' in the plots) with all other coefficients fixed to zero, and one in which those two coefficients are scanned while the remaining WCs are profiled (black dashed-line contour, labelled as 'comb-profiled' in the plots). The best-fit point (BFP) is indicated in each case. In table 5 of section B we list all the 95% CL bounds obtained on each of the five WCs. Finally, we note that all our upcoming results-including $gg \to H$ results- are obtained using the NDR scheme.

We observe that, in the linear case of figure 4, the comb-2D fit yields smaller and differently shaped contours than those obtained from the individual channels. This illustrates that the inclusion of additional production modes provides complementary information and strengthens the overall constraints. By contrast, the comb-profiled contours display

[5]The SMEFiT database can be found here: https://github.com/LHCfitNikhef/smefit_database/.

JHEP01(2026)025

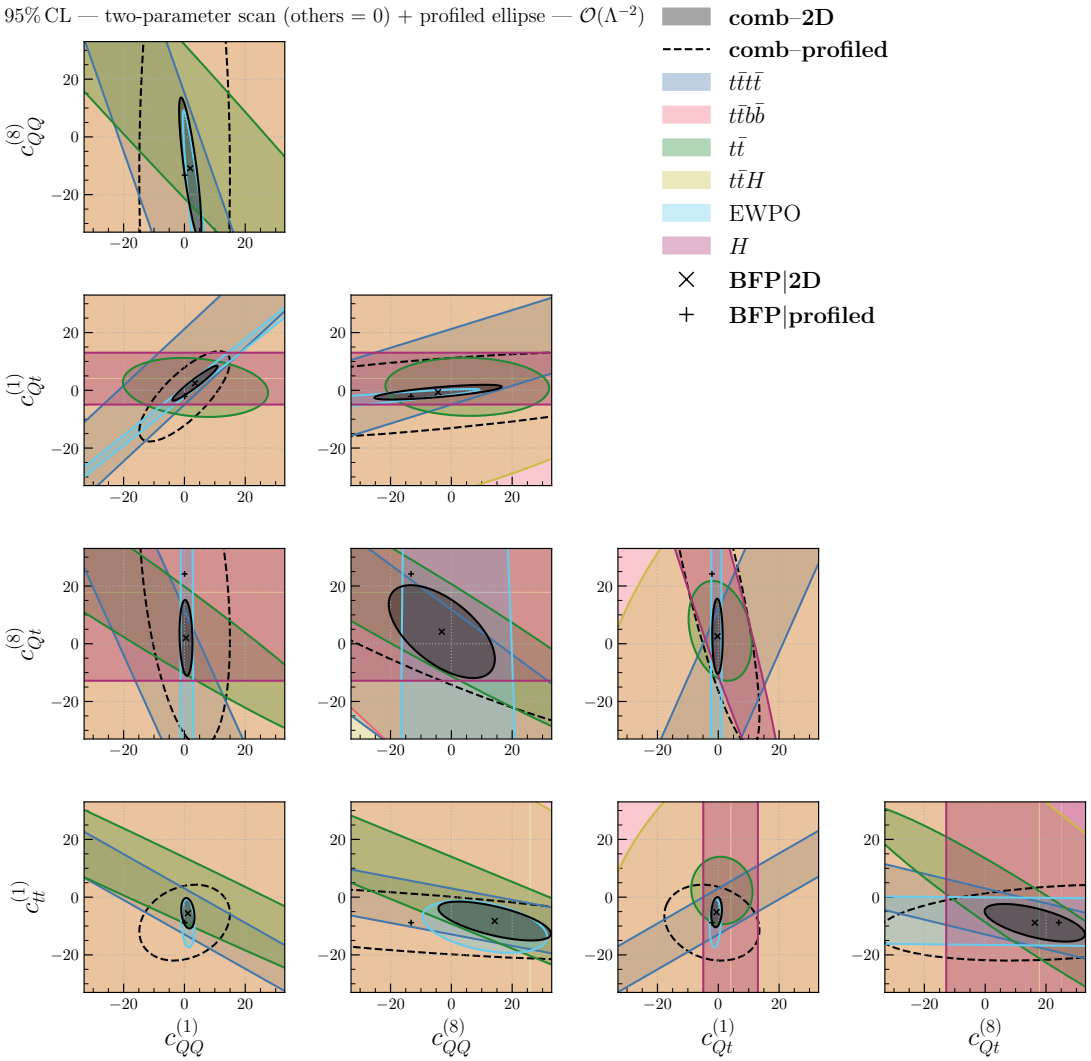

Figure 4. Two-dimensional fits for the four-heavy operator coefficients. Shown are the constraints from each set of observables separately and their combination. Only linear terms, $\mathcal{O}(\Lambda^{-2})$, in the EFT parametrisation are included. The best-fit point (BFP) for the combined fit is indicated for both the two-parameter scan and the profiled scan.

significantly weaker constraining power in comparison to the comb-2D ones, underscoring the impact of the profiled coefficients. Examining at individual datasets, we observe that most are plagued by flat directions; four-top-quark production, for example, shows flat directions for all coefficient pairs we consider. Top-quark pair production in association with a Higgs and $t\bar{t}b\bar{b}$ seem to exhibit the least constraining power among the different processes. Inclusive Higgs production probes only a subset of the coefficients and also has no significant impact on the final combination.

Furthermore, we observe a sizeable impact of the two-loop corrections in our EWPO fit — particularly when compared with the corresponding one-loop contours of ref. [24]. These effects are driven mainly by the non-negligible two-loop contributions to the asymmetry observables A_b and $A_{b,\mathrm{FB}}$; see section C for a detailed comparison between the one- and

JHEP01(2026)025

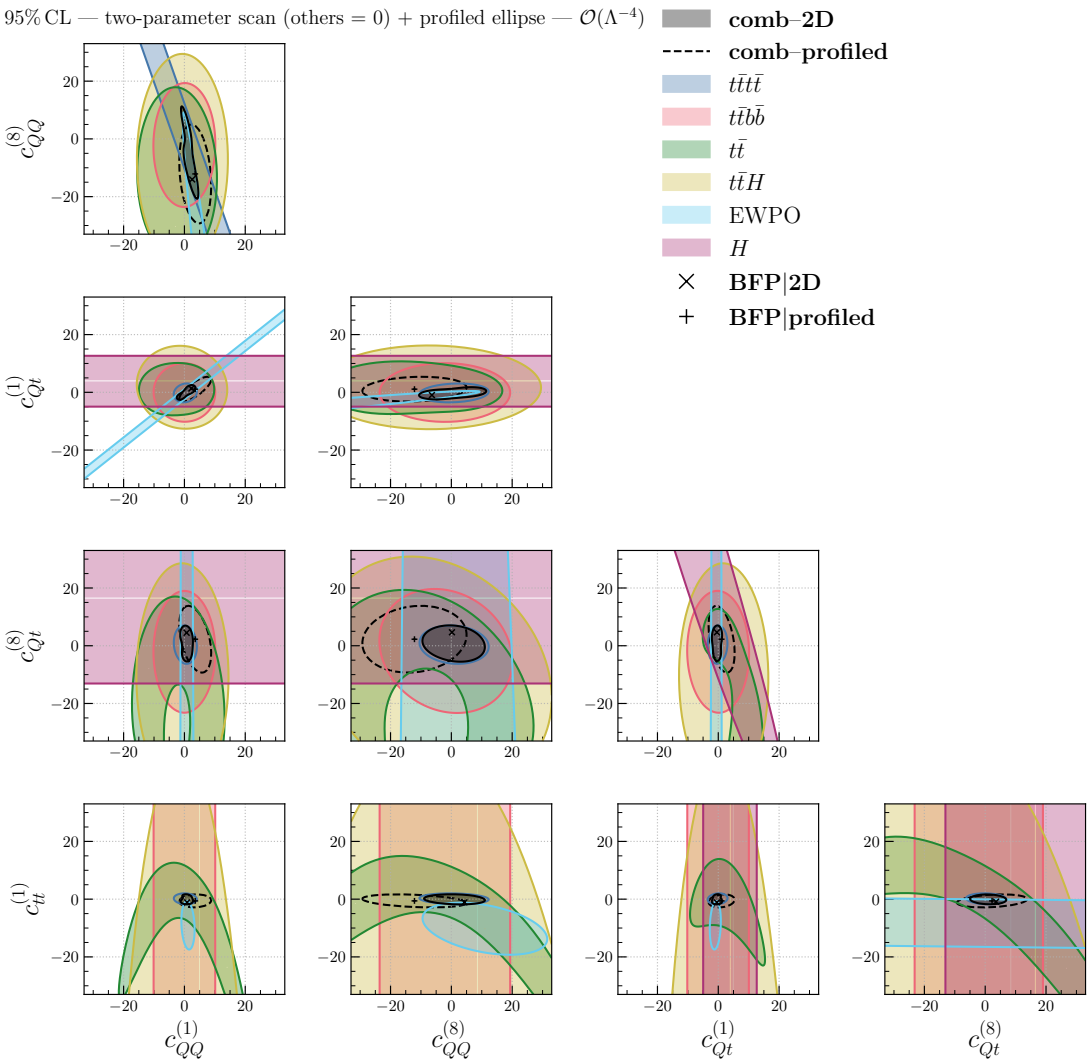

Figure 5. Same as figure 4, but including quadratic terms, $\mathcal{O}(\Lambda^{-4})$, in the EFT parametrisation.

two-loop results for these quantities. We find that the combination of EWPO, top-quark pair and four-top-quark production significantly reduces the allowed parameter space. For some pairs we note that the contours extracted from the EWPO do not include the SM at the 95% CL. This is related to the well-known discrepancy between the measurement of $A_{b,\mathrm{FB}}$ and its SM prediction [83].

At the quadratic level of figure 5, the combined fit yields markedly tighter bounds, driven predominantly by the four-top-quark measurements. The comb-2D contour lies very close to the four-top-quark one, with modest additional tightening from the EWPO. Moreover, the discrepancy between the comb-profiled and comb-2D contours is less pronounced than in the linear case. The most significant reduction in the allowed parameter space appears in the $(c_{QQ}^{(8)}$–$c_{QQ}^{(1)})$ plane, where the four-top-quark channel alone exhibits an almost blind direction; here the EWPO combination is essential to lift the degeneracy.

JHEP01(2026)025

6 Conclusion

In this work we explored how various classes of observables can shed light on the dimension-six four-heavy-quark operators. These operators are notoriously difficult to constrain: global EFT fits typically leave them essentially undetermined at the linear level. To overcome this, several studies have examined loop-induced effects in specific observables, which offer complementary sensitivity to these otherwise elusive interactions.

In particular, we have explored the tree-level contributions of the four-heavy operators to four-top-quark production at the LHC; their one-loop contributions to top-quark pair production and to associated Higgs production-both inclusive and differentially; the two-loop contributions to single-Higgs production in gluon fusion and its subsequent decays; and the one- and two-loop contributions to EWPO. We presented results for all these channels at linear and, where available, quadratic terms in the EFT expansion.

In the case of single-Higgs production via gluon fusion and its subsequent decays, we scrutinised the dependence of the results on the choice of the prescription for the continuation of γ_5 to $d = 4 - 2\epsilon$. We show that this scheme dependence numerically propagates into the bounds on the WCs. Therefore, one must exercise caution when interpreting these limits. Indeed, by restricting the analysis to four-top-quark operators, this assumption leads to a different interpretation of the fit in the BMHV scheme compared with NDR. Establishing a coherent correspondence between the two schemes therefore necessitates the inclusion of additional operators. We defer a full global fit in the BMHV scheme to future work, as our restricted fit clearly calls for a global picture including a full basis of operators.

Finally, we performed a fit combining experimental data from the LHC and LEP, incorporating all relevant theoretical and experimental uncertainties. This allowed us to identify the most sensitive observables and to elucidate the complementarity between tree- and loop-level probes. In the linear fit, the synergy between heavy-quark production and EWPO is key to reducing the allowed parameter space. In the quadratic fit, the strongest constraints arise from four-top-quark production, with the EWPO further reducing the allowed parameter space and lifting degeneracies where present. Moreover, we observed non-negligible two-loop effects in the EWPO fit, predominantly driven by the sizeable two-loop corrections to the asymmetry observables.

In conclusion, we note that a comprehensive assessment of the impact of the observables considered in this work requires their inclusion in a global fit together with the complete set of relevant operators. It is also worthwhile to investigate UV-complete theories which, upon matching onto the EFT, reproduce the operator basis examined here.

Acknowledgments

HF thanks Uli Haisch for helpful discussions and for clarifying technical details of ref. [20]; Víctor Miralles for discussions on the fit method; Marion Thomas for her input on the EWPO implementation; and Giuseppe Ventura for discussions on the γ_5 prescriptions. SDN and RG would like to thank Pablo Olgoso for various discussions on γ_5. EV thanks Gauthier Durieux for valuable discussions on the SMEFT-basis arguments presented in section 2.2. The work of HF and EV is supported by the European Research Council (ERC) under the European Union's Horizon 2020 research and innovation programme (Grant Agreement No. 949451)

JHEP01(2026)025

and by a Royal Society University Research Fellowship (Grant URF/R1/201553). The work of RG is supported in part by the Italian MUR Departments of Excellence grant 2023-2027 "Quantum Frontiers", by the INFN Iniziativa Specifica APINE and by the University of Padua under the 2023 STARS Grants@Unipd programme (Acronym and title of the project: HiggsPairs — Precise Theoretical Predictions for Higgs pair production at the LHC). The research of SDN and MV is supported by the Deutsche Forschungsgemeinschaft (DFG, German Research Foundation) under grant 396021762 — TRR 257 "Particle Physics Phenomenology after the Higgs Discovery".

A Matrix elements for ggH and $\gamma\gamma H$

In this appendix we provide the explicit expression for the auxiliary quantities appearing in eqs. (3.2) and (3.5). We also include the contribution from the operators

$$\begin{aligned}\mathcal{O}_{t\varphi} \equiv \mathcal{Q}_{u\varphi}^{(33)} = (\bar{q}_3\tilde{\varphi}u_3)\left(\varphi^\dagger\varphi\right), \quad \mathcal{O}_{tG} \equiv \mathcal{Q}_{uG}^{(33)} = \bar{q}_3\tilde{\varphi}\sigma^{\mu\nu}T^A u_3 G^A_{\mu\nu},\\ \mathcal{O}_{\varphi G} \equiv \mathcal{Q}_{\varphi G} = G^{A,\mu\nu}G^A_{\mu\nu}\left(\varphi^\dagger\varphi\right),\end{aligned} \tag{A.1}$$

which are required to obtain a result that is independent of the γ_5 continuation scheme. We note that the operator $\mathcal{O}_{\varphi G}$ is introduced to renormalise the one-loop contribution from $\mathcal{O}_{tG}$. We note that the results presented here employ the $\overline{\text{MS}}$ renormalisation scheme for the WCs and the on-shell scheme for the top-quark mass, in contrast to ref. [22], where all parameters were renormalised in the MS scheme.

The matrix element for the process $gg \to H$ (or, equivalently, $H \to gg$) reads

$$\begin{aligned}\mathcal{M}_{\text{OS}}^{ggH} = \frac{c_{\varphi G}}{\Lambda^2}\mathcal{M}_{\varphi G}^{ggH} + \left[c_{tG} + \left(c_{Qt}^1 + \left(c_F - \frac{c_A}{2}\right)c_{Qt}^8\right)\mathcal{K}_{tG}\right]\frac{1}{\Lambda^2}\mathcal{M}_{tG}^{ggH}\\ + \left[1 + \left(c_{Qt}^1 + c_F c_{Qt}^8\right)\frac{1}{\Lambda^2}\left(B_{ggH} + \mathcal{K}_{t\varphi}\right) - \frac{v^3}{\sqrt{2}m_t\,\Lambda^2}c_{t\varphi}\right]\mathcal{M}_{\text{SM}}^{ggH},\end{aligned} \tag{A.2}$$

where c_A and c_F are the SU(N) Casimir invariants in the adjoint and fundamental representations, respectively. For SU(3)$_\text{C}$ they take the values $c_A = 3$ and $c_F = 4/3$. The factor B_{ggH} is defined in eq. (3.4).

The matrix elements entering eq. (A.2) are

$$\begin{aligned}\mathcal{M}_{tG}^{ggH} = -T_F\frac{g_s m_t}{\sqrt{2}\pi^2}L^{\mu_1\mu_2}\epsilon_{\mu_1}(p_1)\epsilon_{\mu_2}(p_2)\delta^{A_1A_2}\times\\ \left(\frac{m_t^2}{m_H^2}\log^2\left(\frac{\beta-1}{\beta+1}\right) + \sqrt{1-\frac{4m_t^2}{m_H^2}}\log\left(\frac{\beta-1}{\beta+1}\right) + 2\log\left(\frac{\mu_R^2}{m_t^2}\right) + 1\right),\end{aligned} \tag{A.3}$$

$$\mathcal{M}_{\text{SM}}^{ggH} = T_F\frac{g_s^2 m_t^2}{4\pi^2 v m_H^2}L^{\mu_1\mu_2}\epsilon_{\mu_1}(p_1)\epsilon_{\mu_2}(p_2)\delta^{A_1A_2}\times\left(\frac{m_H^2 - 4m_t^2}{m_H^2}\log^2\left(\frac{\beta-1}{\beta+1}\right) - 4\right), \tag{A.4}$$

$$\mathcal{M}_{\varphi G}^{ggH} = -4ivL^{\mu_1\mu_2}\epsilon_{\mu_1}(p_1)\epsilon_{\mu_2}(p_2)\delta^{A_1A_2}. \tag{A.5}$$

Here T_F is the Dynkin index of the fundamental representation of SU(N). The Lorentz structure of the amplitude is

$$L^{\mu_1\mu_2} = (m_H^2/2\; g^{\mu_1\mu_2} - p_1^{\mu_2}p_2^{\mu_1}), \tag{A.6}$$

with p_1 and p_2 being the gluon momenta. The indices A_1 and A_2 denote the gluon colour indices.

JHEP01(2026)025

The scheme dependence arising from the two-loop contributions of four-top-quark operators, parametrised by $\mathcal{K}_{tG}$, and $\mathcal{K}_{t\varphi}$ in eq. (3.3), can be compensated by assuming the WCs of operators entering at one loop order are scheme dependent. In particular, the relations

$$c_{t\varphi}^{\text{NDR}} = c_{t\varphi}^{\text{BMHV}} + \left(c_{Qt}^{1} + c_F c_{Qt}^{8}\right) \frac{y_t(\lambda - y_t^2)}{8\pi^2}, \tag{A.7}$$

$$c_{tG}^{\text{NDR}} = c_{tG}^{\text{BMHV}} - \left(c_{Qt}^{1} + \left(c_F - \frac{c_A}{2}\right) c_{Qt}^{8}\right) \frac{y_t g_s}{16\pi^2}, \tag{A.8}$$

render the prediction in eq. (A.2) scheme independent. In these expressions, y_t is the top-quark Yukawa coupling and $\lambda = m_H^2/(2v^2)$. We note that some of the shifts depend on the strong coupling constant, g_s, and thus on the renormalisation scale. This scale dependence must be accounted for when a dynamical scale choice is employed in the calculation.

We now present the matrix element for the Higgs-photon coupling. We use $F^{\mu\nu}$ to denote the photon field strength tensor and introduce the operators $\mathcal{O}_{t\gamma} = (\bar{t}_L \sigma^{\mu\nu} t_R)\frac{H+v}{\sqrt{2}} F_{\mu\nu}$ and $\mathcal{O}_{\varphi\gamma} = HvF^{\mu\nu}F_{\mu\nu}$. These operators are not part of the Warsaw basis, as they are defined directly in terms of the physical fields in the broken phase. Their expression in Warsaw-basis operators can be found in refs. [110, 111]. We finally obtain

$$\begin{aligned}\mathcal{M}_{\text{OS}}^{\gamma\gamma H} = \mathcal{M}_{\text{SM},W}^{\gamma\gamma H} + \frac{c_{\varphi\gamma}}{\Lambda^2}\mathcal{M}_{\varphi\gamma} + \left[c_{t\gamma} + \left(c_{Qt}^{1} + c_F c_{Qt}^{8}\right)\mathcal{K}_{tG}\frac{Q_t e}{g_s}\right]\frac{1}{\Lambda^2}\mathcal{M}_{t\gamma}^{\gamma\gamma H} \\ + \left[1 + \left(c_{Qt}^{1} + c_F c_{Qt}^{8}\right)\frac{1}{\Lambda^2}\left(B_{ggH} + \mathcal{K}_{t\varphi}\right) - \frac{v^3}{\sqrt{2}m_t\,\Lambda^2}c_{t\varphi}\right]\mathcal{M}_{\text{SM}}^{\gamma\gamma H}.\end{aligned} \tag{A.9}$$

The one-loop matrix element for $H \to \gamma\gamma$ can be obtained from that for $H \to gg$ by making the substitutions $g_s \to eQ_t$ and $T_F\delta^{A_1A_2} \to N_C$ in $\mathcal{M}_{tG}^{ggH}$, $\mathcal{M}_{\text{SM}}^{ggH}$, where e is the electric charge of the electron and $Q_t = 2/3$ is the quantised charge of the top quark. We denote the matrix elements of the Higgs boson decay into photons as $\mathcal{M}_{t\gamma}^{\gamma\gamma H}$, $\mathcal{M}_{\text{SM}}^{\gamma\gamma H}$. The tree-level insertion of $\mathcal{O}_{\varphi\gamma}$ is given by $\mathcal{M}_{\varphi\gamma}^{\gamma\gamma H} = -4ivL^{\mu_1\mu_2}\epsilon_{\mu_1}(p_1)\epsilon_{\mu_2}(p_2)$. Regarding the two-loop matrix elements, each four-top-quark operator insertion generates two different colour contractions. We are able to obtain our result from the Higgs-gluon coupling since in the diagrams in figure 2, the only non-vanishing term features a single Dirac trace, allowing the colour structures to be identified unambiguously.

For completeness, the SM contribution to $H \to \gamma\gamma$ with W-boson loops reads

$$\mathcal{M}_{\text{SM},W}^{\gamma\gamma H} = \frac{e^2}{4\pi^2 v}\left(\frac{6m_W^2}{m_H^2} + \left(\frac{6m_W^4}{m_H^4} - \frac{3m_W^2}{m_H^2}\right)\log^2\left(\frac{\beta_W - 1}{\beta_W + 1}\right) + 1\right), \tag{A.10}$$

where $\beta_W = \sqrt{1 - \frac{4m_W^2}{m_H^2}}$.

To render the Higgs decay into photons scheme-independent, we must employ eq. (A.7) with the relation analogous to eq. (A.8), namely

$$c_{t\gamma}^{\text{NDR}} = c_{t\gamma}^{\text{BMHV}} - eQ_t\frac{y_t\left(c_{Qt}^{1} + c_F c_{Qt}^{8}\right)}{8\pi^2}. \tag{A.11}$$

JHEP01(2026)025

	$d\sigma_{\rm NLO}/dp_T^H$ [pb]					
	$p_T^H < 60$ GeV	$60 \le p_T^H < 120$ GeV	$120 \le p_T^H < 200$ GeV	$200 \le p_T^H < 300$ GeV	$300 \le p_T^H < 450$ GeV	$p_T^H \ge 450$ GeV
SM	1.197e−1 ± 0.054%$^{+6\%}_{-9.08\%}$	1.785e−1 ± 0.052%$^{+5.94\%}_{-9.17\%}$	1.258e−1 ± 0.065%$^{+5.97\%}_{-9.43\%}$	5.203e−2 ± 0.096%$^{+5.47\%}_{-9.61\%}$	1.888e−2 ± 0.141%$^{+3.36\%}_{-9.24\%}$	5.179e−3 ± 0.28%$^{+1.76\%}_{-6.8\%}$
			$\mathcal{O}(c_i/\Lambda^2)$			
c_{tt}^1	−3.693e−5 ± 1.878%$^{+55.11\%}_{-34.6\%}$	−1.173e−4 ± 0.867%$^{+49.39\%}_{-31.81\%}$	−1.223e−4 ± 1.11%$^{+56.16\%}_{-35.46\%}$	1.134e−6 ± 139%$^{+1632\%}_{-2106\%}$	9.791e−5 ± 1.872%$^{+21.88\%}_{-18.05\%}$	1.567e−4 ± 1.387%$^{+31.86\%}_{-22.53\%}$
c_{QQ}^1	−9.997e−5 ± 1.227%$^{+36.9\%}_{-25.25\%}$	−1.911e−4 ± 0.96%$^{+38.41\%}_{-26.06\%}$	−1.63e−4 ± 1.896%$^{+42.95\%}_{-28.45\%}$	−4.519e−5 ± 6.025%$^{+64.81\%}_{-39.8\%}$	3.056e−5 ± 9.49%$^{+32.56\%}_{-28.18\%}$	7.125e−5 ± 5.559%$^{+31.13\%}_{-22.19\%}$
c_{QQ}^8	2.735e−5 ± 3.993%$^{+11.41\%}_{-14.46\%}$	5.53e−5 ± 3.214%$^{+9.25\%}_{-13.25\%}$	8.329e−5 ± 2.527%$^{+13.33\%}_{-13.98\%}$	8.667e−5 ± 2.701%$^{+15.39\%}_{-12.49\%}$	8.205e−5 ± 3.134%$^{+24.33\%}_{-17.51\%}$	7.729e−5 ± 4.074%$^{+32.33\%}_{-22.3\%}$
c_{Qt}^1	−1.262e−3 ± 0.246%$^{+31.97\%}_{-22.67\%}$	−1.93e−3 ± 0.203%$^{+32.61\%}_{-22.98\%}$	−1.338e−3 ± 0.258%$^{+33.74\%}_{-23.52\%}$	−4.837e−4 ± 0.553%$^{+34.96\%}_{-24.05\%}$	−1.277e−4 ± 1.555%$^{+34.69\%}_{-23.78\%}$	−3.17e−5 ± 6.399%$^{+31.59\%}_{-22.27\%}$
c_{Qt}^8	−1.149e−4 ± 1.008%$^{+39.12\%}_{-28.69\%}$	−1.266e−4 ± 1.521%$^{+45.7\%}_{-33.33\%}$	3.364e−6 ± 74.484%$^{+389\%}_{-535\%}$	9.672e−5 ± 2.479%$^{+20.53\%}_{-14.5\%}$	1.129e−4 ± 2.405%$^{+28.3\%}_{-19.84\%}$	1.088e−4 ± 3.605%$^{+33.57\%}_{-23.02\%}$
			$\mathcal{O}(c_i^2/\Lambda^4)$			
c_{tt}^1	×	×	×	×	×	×
c_{QQ}^1	2.89e−5 ± 2.048%$^{+4.14\%}_{-5.08\%}$	5.913e−5 ± 1.867%$^{+4.61\%}_{-4.27\%}$	6.764e−5 ± 1.804%$^{+4.94\%}_{-3.84\%}$	5.253e−5 ± 2.259%$^{+6.82\%}_{-4.48\%}$	3.687e−5 ± 3.338%$^{+8.42\%}_{-5.56\%}$	2.779e−5 ± 4.385%$^{+8.37\%}_{-5.23\%}$
c_{QQ}^8	4.415e−6 ± 3.202%$^{+8.53\%}_{-5.52\%}$	8.902e−6 ± 2.504%$^{+7.99\%}_{-4.62\%}$	1.034e−5 ± 2.034%$^{+9.56\%}_{-5.3\%}$	8.285e−6 ± 2.89%$^{+10.59\%}_{-5.96\%}$	5.831e−6 ± 4.934%$^{+12\%}_{-6.83\%}$	4.937e−6 ± 6.78%$^{+14.48\%}_{-8.38\%}$
c_{Qt}^1	2.833e−5 ± 1.938%$^{+4.06\%}_{-5.02\%}$	6.055e−5 ± 1.45%$^{+4.17\%}_{-5.06\%}$	6.545e−5 ± 1.927%$^{+5.11\%}_{-3.51\%}$	5.113e−5 ± 2.355%$^{+6.15\%}_{-3.97\%}$	3.639e−5 ± 3.024%$^{+7.48\%}_{-4.79\%}$	3.042e−5 ± 4.135%$^{+12.52\%}_{-8.65\%}$
c_{Qt}^8	4.303e−6 ± 3.461%$^{+8.26\%}_{-5.78\%}$	8.2e−6 ± 2.807%$^{+8.72\%}_{-6.28\%}$	1.01e−5 ± 2.563%$^{+9.22\%}_{-5.09\%}$	7.497e−6 ± 7.655%$^{+11.93\%}_{-7.69\%}$	4.598e−6 ± 11.933%$^{+15.1\%}_{-13.59\%}$	4.561e−6 ± 8.879%$^{+12.56\%}_{-6.43\%}$
			$\mathcal{O}(c_i c_j/\Lambda^4)$			
$c_{QQ}^1 c_{Qt}^1$	1.49e−5 ± 8.241%$^{+8.56\%}_{-6.91\%}$	2.817e−5 ± 7.635%$^{+9.7\%}_{-8.02\%}$	2.928e−5 ± 9.17%$^{+10.63\%}_{-6.63\%}$	1.762e−5 ± 14.089%$^{+10.58\%}_{-6.63\%}$	1.086e−5 ± 21.595%$^{+8.73\%}_{-8.76\%}$	−2.153e−6 ± 118%$^{+62.83\%}_{-68.99\%}$
$c_{QQ}^8 c_{Qt}^8$	3.253e−6 ± 11.559%$^{+2.76\%}_{-5.77\%}$	5.878e−6 ± 10.101%$^{+10.34\%}_{-13.75\%}$	7.997e−6 ± 7.513%$^{+4.73\%}_{-6.71\%}$	4.398e−6 ± 19.689%$^{+9.78\%}_{-12.84\%}$	4.704e−6 ± 18.524%$^{+5.68\%}_{-1.91\%}$	6.259e−7 ± 123%$^{+109\%}_{-122\%}$

Table 2. Differential p_T^H predictions in the SM and SMEFT in the $t\bar{t}H$ process. The cross sections are reported as the integral within the bin range. The uncertainties quoted correspond, respectively, to the Monte Carlo statistical uncertainty and the QCD scale uncertainty from a 9-point variation.

B Numerical predictions

Table 2 presents the differential p_T^H spectrum in the ATLAS $t\bar{t}H$ bins, whilst table 3 lists the inclusive cross sections for all top-quark processes. SMEFT results are split into interference, quadratic, and cross terms, with total-rate K-factors given. All WCs are set to unity and $\Lambda = 1$ TeV. Predictions are quoted within their QCD scale uncertainties and MC statistical errors. Predictions which are compatible with zero within a MC error of 2σ or greater are omitted and denoted by the '-'. The 'x' indicates no contribution from the corresponding operator.

Table 4 lists our numerical predictions for single-Higgs production and for Higgs decays into gluons and photons. The quoted SM value is the LO result with only top- and W-boson loops included. Quadratic SMEFT terms are strongly suppressed relative to the linear ones and are therefore not shown.

C EWPO

We employ the relations in eq. (C.1) where the WCs C_{HD} and C_{HWB} are expressed in terms of the shifts to the oblique parameters S and T [19] and in terms of the shifts of the

JHEP01(2026)025

	$\sigma^{\text{proc.}}_{\text{(N)LO}}$ [pb]						
	$\sigma^{t\bar{t}}_{\text{LO}}$	$\sigma^{t\bar{t}}_{\text{NLO}}$	$K_{t\bar{t}}$	$\sigma^{t\bar{t}H}_{\text{LO}}$	$\sigma^{t\bar{t}H}_{\text{NLO}}$	$K_{t\bar{t}H}$	$\sigma^{t\bar{t}t\bar{t}}_{\text{LO}}$
SM	$5.028\text{e+}2 \pm 0.003\%^{+29.67\%}_{-21.44\%}$	$7.532\text{e+}2 \pm 0.004\%^{+11.75\%}_{-11.9\%}$	1.498	$4.005\text{e}{-1} \pm 0.005\%^{+31.45\%}_{-22.25\%}$	$5.003\text{e}{-1} \pm 0.009\%^{+5.71\%}_{-9.24\%}$	1.249	$6.754\text{e}{-3} \pm 0.016\%^{+62.66\%}_{-35.48\%}$
				$\mathcal{O}(c_i/\Lambda^2)$			
c^1_{tt}	×	$2.376\text{e}{-1} \pm 0.461\%^{+24.03\%}_{-18.41\%}$	×	×	$-2.089\text{e}{-5} \pm 17.867\%^{+494\%}_{-339\%}$	×	$-1.185\text{e}{-3} \pm 0.026\%^{+36.07\%}_{-24.93\%}$
c^1_{QQ}	×	$-3.323\text{e}{-2} \pm 1.731\%^{+53.94\%}_{-34.92\%}$	×	×	$-3.975\text{e}{-4} \pm 1.688\%^{+46.88\%}_{-30.48\%}$	×	$-7.053\text{e}{-4} \pm 0.024\%^{+37.35\%}_{-25.48\%}$
c^8_{QQ}	$5.961\text{e}{-2} \pm 0.123\%^{+27.97\%}_{-25.65\%}$	$1.209\text{e}{-1} \pm 0.406\%^{+10.94\%}_{-12.13\%}$	2.028	$1.708\text{e}{-4} \pm 0.393\%^{+22.3\%}_{-21.22\%}$	$4.119\text{e}{-4} \pm 1.3\%^{+12.4\%}_{-11.31\%}$	2.411	$-2.351\text{e}{-4} \pm 0.027\%^{+37.39\%}_{-25.50\%}$
c^1_{Qt}	×	$-2.538 \pm 0.053\%^{+29.22\%}_{-21.29\%}$	×	×	$-5.175\text{e}{-3} \pm 0.138\%^{+33.01\%}_{-23.16\%}$	×	$7.191\text{e}{-4} \pm 0.024\%^{+41.42\%}_{-27.19\%}$
c^8_{Qt}	$5.951\text{e}{-2} \pm 0.135\%^{+27.97\%}_{-25.65\%}$	$-1.116\text{e}{-1} \pm 0.48\%^{+37.42\%}_{-30.59\%}$	1.875	$1.702\text{e}{-4} \pm 0.464\%^{+22.28\%}_{-21.21\%}$	$8.029\text{e}{-5} \pm 7.662\%^{+33.34\%}_{-40.45\%}$	0.471	$-3.026\text{e}{-4} \pm 0.029\%^{+29.98\%}_{-22.35\%}$
				$\mathcal{O}(c_i^2/\Lambda^4)$			
c^1_{tt}	×	×	×	×	×	×	$4.342\text{e}{-3} \pm 0.021\%^{+46.06\%}_{-29.23\%}$
c^1_{QQ}	$2.739\text{e}{-2} \pm 0.233\%^{+13.52\%}_{-16.73\%}$	$5.863\text{e}{-2} \pm 0.378\%^{+6.51\%}_{-7.68\%}$	2.14	$1.608\text{e}{-4} \pm 0.686\%^{+9.34\%}_{-12.45\%}$	$2.728\text{e}{-4} \pm 0.84\%^{+5.9\%}_{-3.77\%}$	1.696	$1.085\text{e}{-3} \pm 0.029\%^{+46\%}_{-29.19\%}$
c^8_{QQ}	$6.061\text{e}{-3} \pm 0.3\%^{+13.53\%}_{-16.74\%}$	$1.029\text{e}{-2} \pm 0.365\%^{+6.82\%}_{-4.65\%}$	1.697	$3.579\text{e}{-5} \pm 0.826\%^{+9.33\%}_{-12.44\%}$	$4.271\text{e}{-5} \pm 1.275\%^{+10.23\%}_{-5.71\%}$	1.193	$1.208\text{e}{-4} \pm 0.045\%^{+45.98\%}_{-29.18\%}$
c^1_{Qt}	$2.73\text{e}{-2} \pm 0.266\%^{+13.54\%}_{-16.75\%}$	$5.877\text{e}{-2} \pm 0.378\%^{+6.68\%}_{-7.78\%}$	2.152	$1.616\text{e}{-4} \pm 0.614\%^{+9.31\%}_{-12.42\%}$	$2.722\text{e}{-4} \pm 0.789\%^{+5.96\%}_{-3.8\%}$	1.684	$1.47\text{e}{-3} \pm 0.048\%^{+46.21\%}_{-29.28\%}$
c^8_{Qt}	$6.047\text{e}{-3} \pm 0.32\%^{+13.53\%}_{-16.74\%}$	$9.186\text{e}{-3} \pm 0.77\%^{+9.22\%}_{-6.16\%}$	1.519	$3.597\text{e}{-5} \pm 0.982\%^{+9.29\%}_{-12.41\%}$	$3.926\text{e}{-5} \pm 2.326\%^{+10.61\%}_{-6.52\%}$	1.091	$3.545\text{e}{-4} \pm 0.055\%^{+45.89\%}_{-29.15\%}$
				$\mathcal{O}(c_i c_j/\Lambda^4)$			
$c^1_{QQ}c^1_{Qt}$	$1.41\text{e}{-2} \pm 0.778\%^{+15.62\%}_{-18.47\%}$	$1.128\text{e}{-2} \pm 3.178\%^{+11.8\%}_{-10.75\%}$	0.8	$1.585\text{e}{-4} \pm 1.231\%^{+10.1\%}_{-13.13\%}$	$9.87\text{e}{-5} \pm 4.431\%^{+11.21\%}_{-7.92\%}$	0.622	$-3.51\text{e}{-4} \pm 0.261\%^{+43.39\%}_{-28.12\%}$
$c^1_{QQ}c^1_{tt}$	–	–	×	–	–	×	$3.566\text{e}{-4} \pm 0.365\%^{+41.6\%}_{-27.33\%}$
$c^1_{QQ}c^8_{QQ}$	–	$1.066\text{e}{-3} \pm 23.367\%^{+24.19\%}_{-23.49\%}$	×	–	–	×	$7.241\text{e}{-4} \pm 0.072\%^{+46.07\%}_{-29.23\%}$
$c^1_{QQ}c^8_{Qt}$	–	–	×	–	–	×	$1.314\text{e}{-4} \pm 0.381\%^{+42.77\%}_{-27.84\%}$
$c^1_{Qt}c^1_{tt}$	–	$5.545\text{e}{-4} \pm 45.484\%^{+14.2\%}_{-16.01\%}$	×	–	–	×	$-7.075\text{e}{-4} \pm 0.202\%^{+43.31\%}_{-28.07\%}$
$c^1_{Qt}c^8_{QQ}$	–	–	×	–	–	×	$-1.18\text{e}{-4} \pm 0.723\%^{+43.31\%}_{-28.06\%}$
$c^1_{Qt}c^8_{Qt}$	–	$-2.956\text{e}{-3} \pm 9.905\%^{+28.22\%}_{-26.3\%}$	×	–	$-1.689\text{e}{-5} \pm 19.597\%^{+23.96\%}_{-23.82\%}$	×	$-8.382\text{e}{-5} \pm 1.078\%^{+41.67\%}_{-27.38\%}$
$c^1_{tt}c^8_{QQ}$	–	–	×	–	$1.931\text{e}{-6} \pm 37.788\%^{+26.67\%}_{-25.98\%}$	×	$1.181\text{e}{-4} \pm 1.002\%^{+41.56\%}_{-27.31\%}$
$c^1_{tt}c^8_{Qt}$	–	$4.615\text{e}{-4} \pm 16.652\%^{+30.32\%}_{-27.57\%}$	×	–	–	×	$2.603\text{e}{-4} \pm 0.461\%^{+42.62\%}_{-27.77\%}$
$c^8_{QQ}c^8_{Qt}$	$3.177\text{e}{-3} \pm 0.965\%^{+15.56\%}_{-18.42\%}$	$3.907\text{e}{-3} \pm 2.285\%^{+2.25\%}_{-3.99\%}$	1.229	$3.45\text{e}{-5} \pm 2.034\%^{+10.22\%}_{-13.24\%}$	$2.685\text{e}{-5} \pm 5.113\%^{+7.94\%}_{-10.45\%}$	0.778	$4.391\text{e}{-5} \pm 0.584\%^{+42.65\%}_{-27.77\%}$

Table 3. Inclusive predictions for top-quark processes in the SM and SMEFT.

JHEP01(2026)025

	$\sigma_{\rm int}$ [pb]
	$\mathcal{O}(c_i/\Lambda^2)$
c_{Qt}^1 (NDR)	-0.3203
c_{Qt}^8 (NDR)	-0.1033
c_{Qt}^1 (BMHV)	-0.0830
c_{Qt}^8 (BMHV)	-0.1106
$\sigma_{\rm SM}$	16.51 pb

(a) $gg \to H$ cross section.

	$\Gamma_{\rm int}$ [MeV]
	$\mathcal{O}(c_i/\Lambda^2)$
c_{Qt}^1 (NDR)	-1.912×10^{-3}
c_{Qt}^8 (NDR)	-4.810×10^{-4}
c_{Qt}^1 (BMHV)	-2.781×10^{-4}
c_{Qt}^8 (BMHV)	-3.708×10^{-4}
$\Gamma_{\rm SM}$	0.1960 MeV

(b) $H \to gg$ partial width.

	$\Gamma_{\rm int}$ [MeV]
	$\mathcal{O}(c_i/\Lambda^2)$
c_{Qt}^1 (NDR)	2.798×10^{-5}
c_{Qt}^8 (NDR)	3.731×10^{-5}
c_{Qt}^1 (BMHV)	4.069×10^{-6}
c_{Qt}^8 (BMHV)	5.426×10^{-6}
$\Gamma_{\rm SM}$	1.016×10^{-2} MeV

(c) $H \to \gamma\gamma$ partial width.

Table 4. Linear EFT contributions and SM values for single-Higgs inclusive production cross section in gluon-fusion channel (table 4(a)) and Higgs decays (tables 4(b) and 4(c)), parametrised as in eq. (2.2). WCs are set to unity with $\Lambda = 1\,\text{TeV}$. The SM values correspond to the LO one-loop result including only the dominant top- and W-loops. Results are presented in both the NDR and the BMHV schemes.

Weinberg angle, s_θ, and the effective couplings [91]. The two-loop contributions to the oblique parameters ΔS and ΔT have been computed in and are taken from ref. [20].

$$\begin{aligned} C_{HD} &= -\frac{2\,\alpha\,\Delta T}{v^2}, \quad C_{HWB} = \frac{\alpha\,\Delta S}{4\,c_\theta\,s_\theta\,v^2}, \\ \delta s_\theta^2 &= \frac{m_W^2\,C_{HD}}{2\sqrt{2}\,G_F\,m_Z^2} + \frac{m_W\,C_{HWB}}{\sqrt{2}\,G_F\,m_Z}\sqrt{1-\frac{m_W^2}{m_Z^2}}, \quad \delta g_Z = -\frac{C_{HD}}{4\sqrt{2}\,G_F}. \end{aligned} \tag{C.1}$$

Using eq. (C.1) and substituting into the shifts in vector and axial-vector couplings shown in eq. (C.2)—which can be found in ref. [91]—we obtain the modified vector and axial-vector couplings due to the effective operators:

$$\begin{aligned} \delta g_V^f &= \delta g_Z\,g_V^f + Q^f\,\delta s_\theta^2\,, \\ \delta g_A^f &= \delta g_Z\,g_A^f\,, \end{aligned} \tag{C.2}$$

where $g_V^f = T_3/2 - Q^f s_\theta^2$ and $g_A^f = T_3/2$, where T_3 is weak isospin and Q^f is the electric charge. We adopt the conventions of ref. [91] and use the following definitions of the EWPO:

$$\begin{aligned} \Gamma_i &= \frac{\sqrt{2}\,G_F\,m_Z^3\,N_c}{3\pi}\,(|g_V^i|^2 + |g_A^i|^2), \\ \Gamma_{\rm had} &= \sum_{q=u,d,c,s,b}\Gamma_q, \qquad R_c = \frac{\Gamma_c}{\Gamma_{\rm had}}, \quad R_b = \frac{\Gamma_b}{\Gamma_{\rm had}}, \quad R_\ell = \frac{\Gamma_{\rm had}}{\Gamma_\ell}. \end{aligned} \tag{C.3}$$

For the numerical analysis we adopt the following input parameters:

$$\begin{aligned} G_F &= 1.166379 \times 10^{-5}\ \text{GeV}^{-2}, & m_W &= 80.379\ \text{GeV}, & m_Z &= 91.1876\ \text{GeV}, \\ v &= 246.22\ \text{GeV}, & \alpha &= 1/132.184, & s_\theta^2 &= 0.2230, \\ c_\theta^2 &= 1 - s_\theta^2, & m_t &= 172.5\ \text{GeV}, & \Lambda &= 1\ \text{TeV}, \\ \mu_R &= m_Z, & \Gamma_Z^{\rm SM} &= 2.4941\ \text{GeV}, & \Gamma_{\rm had}^{\rm SM} &= 1.6944\ \text{GeV}, \\ R_b^{\rm SM} &= 0.21582, & A_b^{\rm SM} &= 0.9347, & A_{b,\rm FB}^{\rm SM} &= 0.1029\,. \end{aligned} \tag{C.4}$$

JHEP01(2026)025

Corrections to Γ_b

Adopting the one-loop result of ref. [20] and including the two-loop contributions as described above, the relative shift in the $Z \to b\bar{b}$ partial width, $\delta\Gamma_b$, reads

$$\begin{aligned}
\delta\Gamma_b^{1L}/\Gamma_Z^{SM} &= (3.8320\, c_{QQ}^1 + 0.4065\, c_{QQ}^8 - 4.5839\, c_{Qt}^1) \times 10^{-4} \\
\delta\Gamma_b^{1L+2L}/\Gamma_Z^{SM} &= (3.8255\, c_{QQ}^1 + 0.4049\, c_{QQ}^8 - 4.5745\, c_{Qt}^1 + 0.0018\, c_{Qt}^8 - 0.0125\, c_{tt}^1) \times 10^{-4},
\end{aligned} \tag{C.5}$$

where $\delta\Gamma_b^{1L}$ and $\delta\Gamma_b^{1L+2L}$ denote the one-loop and the combined one- and two-loop contributions, respectively.

Corrections to R_c, R_ℓ, and R_b

Implementing the above definitions and expanding to first order in $\delta\Gamma_b$, we obtain

$$\bar{R}_c = \frac{\Gamma_c^{SM}}{\Gamma_{had}^{SM} + \delta\Gamma_b} \simeq R_c^{SM}\left(1 - \frac{\delta\Gamma_b}{\Gamma_{had}^{SM}}\right), \quad \bar{R}_\ell = \frac{\Gamma_{had}^{SM} + \delta\Gamma_b}{\Gamma_\ell^{SM}} \simeq R_\ell^{SM}\left(1 + \frac{\delta\Gamma_b}{\Gamma_{had}^{SM}}\right),$$
$$\bar{R}_b = \frac{\Gamma_b^{SM} + \delta\Gamma_b}{\Gamma_{had}^{SM} + \delta\Gamma_b} \simeq R_b^{SM} + (1 - R_b^{SM})\,\frac{\delta\Gamma_b}{\Gamma_{had}^{SM}}\,. \tag{C.6}$$

Replacing $\delta\Gamma_b \to \delta\Gamma_b^{1L}$ or $\delta\Gamma_b^{1L+2L}$ gives

$$\begin{aligned}
\delta R_c^{1L}/R_c^{SM} &= (-5.6404\, c_{QQ}^1 - 0.5983\, c_{QQ}^8 + 6.7472\, c_{Qt}^1) \times 10^{-4} \\
\delta R_c^{1L+2L}/R_c^{SM} &= (-5.6308\, c_{QQ}^1 - 0.5959\, c_{QQ}^8 + 6.7333\, c_{Qt}^1 - 0.0026\, c_{Qt}^8 + 0.0184\, c_{tt}^1) \times 10^{-4}, \\
\delta R_b^{1L}/R_b^{SM} &= (20.494\, c_{QQ}^1 + 2.1742\, c_{QQ}^8 - 24.516\, c_{Qt}^1) \times 10^{-4} \\
\delta R_b^{1L+2L}/R_b^{SM} &= (20.459\, c_{QQ}^1 + 2.1654\, c_{QQ}^8 - 24.465\, c_{Qt}^1 + 0.0096\, c_{Qt}^8 - 0.0669\, c_{tt}^1) \times 10^{-4}.
\end{aligned} \tag{C.7}$$

Corrections to A_b, $A_{b,FB}$

Using the one-loop result of ref. [20], the one-loop shifts read

$$\begin{aligned}
\delta A_b^{1L}/A_b^{SM} &= (2.3648\, c_{QQ}^1 + 0.2508\, c_{QQ}^8 - 2.8288\, c_{Qt}^1) \times 10^{-4} \\
\delta A_{b,FB}^{1L}/A_{b,FB}^{SM} &= (2.3682\, c_{QQ}^1 + 0.2512\, c_{QQ}^8 - 2.8329\, c_{Qt}^1) \times 10^{-4}
\end{aligned} \tag{C.8}$$

where we have used the relation $A_{b,FB} = {}^3\!/_4 A_b A_e$ [112]. Including the two-loop shifts using the following relations [112]:

$$A_e = 2\,\frac{g_V^\ell\, g_A^\ell}{(g_V^\ell)^2 + (g_A^\ell)^2}\,, \qquad A_f = 2\,\frac{g_V^f\, g_A^f}{(g_V^f)^2 + (g_A^f)^2}\,, \tag{C.9}$$

we obtain the total corrections for the asymmetry observables:

$$\begin{aligned}
\delta A_b^{1L+2L}/A_b^{SM} &= (2.6316\, c_{QQ}^1 + 0.3447\, c_{QQ}^8 - 3.1499\, c_{Qt}^1 + 0.0062\, c_{Qt}^8 + 0.6133\, c_{tt}^1) \times 10^{-4}, \\
\delta A_{b,FB}^{1L+2L}/A_{b,FB}^{SM} &= (24.593\, c_{QQ}^1 + 8.0737\, c_{QQ}^8 - 29.576\, c_{Qt}^1 + 0.5198\, c_{Qt}^8 + 51.083\, c_{tt}^1) \times 10^{-4}.
\end{aligned} \tag{C.10}$$

JHEP01(2026)025

	Order	$t\bar{t}H$	$t\bar{t}t\bar{t}$	$t\bar{t}b\bar{b}$	$gg \to H$	$t\bar{t}$	EWPO
c_{tt}^1	$\mathcal{O}(\Lambda^{-2})$	[-79.98, 37.36]	[-11.31, 1.42]	–	–	[-6.94, 11.72]	[-14.92, - 1.68]
	$\mathcal{O}(\Lambda^{-4})$	[-79.98, 37.36]	[-1.62, 1.89]	–	–	[-6.94, 11.72]	[-14.92, - 1.68]
c_{QQ}^1	$\mathcal{O}(\Lambda^{-2})$	–	[-19.00, 2.40]	–	–	[-14.75, 22.89]	[-0.94, 2.49]
	$\mathcal{O}(\Lambda^{-4})$	[-13.20, 11.92]	[-3.20, 3.85]	[-9.31, 9.32]	–	[-14.06, 9.36]	[-0.94, 2.49]
c_{QQ}^8	$\mathcal{O}(\Lambda^{-2})$	–	[-57.01, 7.20]	[-39.53, 91.23]	–	[-16.18, 26.89]	[-13.31, 16.79]
	$\mathcal{O}(\Lambda^{-4})$	[-38.30, 24.08]	[-9.60, 11.55]	[-21.91, 17.67]	–	[-41.86, 17.41]	[-13.31, 16.79]
c_{Qt}^1	$\mathcal{O}(\Lambda^{-2})$	[-26.19, 68.73]	[-2.35, 18.64]	–	[-3.14, 11.23]	[-6.77, 9.34]	[-2.08, 0.78]
	$\mathcal{O}(\Lambda^{-4})$	[-10.40, 13.92]	[-3.27, 2.78]	[-9.39, 9.26]	[-3.16, 10.93]	[-7.27, 9.69]	[-2.08, 0.78]
c_{Qt}^8	$\mathcal{O}(\Lambda^{-2})$	[-117.00, 39.40]	[-44.30, 5.59]	[-38.41, 88.66]	[-6.71, 42.30]	[-8.69, 18.14]	–
	$\mathcal{O}(\Lambda^{-4})$	[-44.52, 22.92]	[-5.73, 6.59]	[-21.56, 17.34]	[-7.06, 39.16]	[-56.11, 19.70]	–

Table 5. 95% CL individual bounds from each process.

	Individual		Marginalised	
	$\mathcal{O}(\Lambda^{-2})$	$\mathcal{O}(\Lambda^{-4})$	$\mathcal{O}(\Lambda^{-2})$	$\mathcal{O}(\Lambda^{-4})$
c_{tt}^1	[-9.12, -0.89]	[-1.66, 1.49]	[-16.30, -1.45]	[-1.50, 1.52]
c_{QQ}^1	[-0.99, 2.41]	[-0.84, 3.03]	[-8.42, 8.50]	[-0.97, 5.94]
c_{QQ}^8	[-11.39, 11.46]	[-8.60, 10.84]	[-75.66, 48.77]	[-19.43, 5.85]
c_{Qt}^1	[-1.74, 1.03]	[-2.30, 1.17]	[-10.99, 6.71]	[-1.37, 2.69]
c_{Qt}^8	[-7.93, 12.88]	[-4.39, 6.63]	[-9.50, 58.36]	[-4.09, 6.20]

Table 6. 95% CL individual and marginalised bounds from the combined fit.

D Additional fit results

We report here the 95% CL bounds on each of the five WCs from each process, summarised in table 5. The corresponding individual and marginalised limits from the combined fit are shown in table 6. All bounds are quoted at both linear and quadratic order in the EFT expansion.

Data Availability Statement. This article has no associated data or the data will not be deposited.

Code Availability Statement. This article has no associated code or the code will not be deposited.

References

[1] J. de Blas et al., *Electroweak precision observables and Higgs-boson signal strengths in the Standard Model and beyond: present and future*, *JHEP* **12** (2016) 135 [arXiv:1608.01509] [INSPIRE].

[2] J. Ellis et al., *Top, Higgs, Diboson and Electroweak Fit to the Standard Model Effective Field Theory*, *JHEP* **04** (2021) 279 [arXiv:2012.02779] [INSPIRE].

JHEP01(2026)025

[3] I. Brivio et al., *From models to SMEFT and back?*, *SciPost Phys.* **12** (2022) 036 [arXiv:2108.01094] [INSPIRE].

[4] SMEFiT collaboration, *Combined SMEFT interpretation of Higgs, diboson, and top quark data from the LHC*, *JHEP* **11** (2021) 089 [arXiv:2105.00006] [INSPIRE].

[5] E. Celada et al., *Mapping the SMEFT at high-energy colliders: from LEP and the (HL-)LHC to the FCC-ee*, *JHEP* **09** (2024) 091 [arXiv:2404.12809] [INSPIRE].

[6] R. Bartocci, A. Biekötter and T. Hurth, *Renormalisation group evolution effects on global SMEFT analyses*, *JHEP* **05** (2025) 203 [arXiv:2412.09674] [INSPIRE].

[7] J. ter Hoeve et al., *Connecting scales: RGE effects in the SMEFT at the LHC and future colliders*, *JHEP* **06** (2025) 125 [arXiv:2502.20453] [INSPIRE].

[8] J. de Blas et al., *Constraining new physics effective interactions via a global fit of electroweak, Drell-Yan, Higgs, top, and flavour observables*, arXiv:2507.06191 [INSPIRE].

[9] ATLAS collaboration, *Observation of four-top-quark production in the multilepton final state with the ATLAS detector*, *Eur. Phys. J. C* **83** (2023) 496 [*Erratum ibid.* **84** (2024) 156] [arXiv:2303.15061] [INSPIRE].

[10] CMS collaboration, *Observation of four top quark production in proton-proton collisions at s=13TeV*, *Phys. Lett. B* **847** (2023) 138290 [arXiv:2305.13439] [INSPIRE].

[11] CMS collaboration, *Measurement of the $t\bar{t}b\bar{b}$ production cross section in the all-jet final state in pp collisions at $\sqrt{s} = 13$ TeV*, *Phys. Lett. B* **803** (2020) 135285 [arXiv:1909.05306] [INSPIRE].

[12] B. Lillie, J. Shu and T.M.P. Tait, *Top Compositeness at the Tevatron and LHC*, *JHEP* **04** (2008) 087 [arXiv:0712.3057] [INSPIRE].

[13] K. Kumar, T.M.P. Tait and R. Vega-Morales, *Manifestations of Top Compositeness at Colliders*, *JHEP* **05** (2009) 022 [arXiv:0901.3808] [INSPIRE].

[14] G. Banelli et al., *The Present and Future of Four Top Operators*, *JHEP* **02** (2021) 043 [arXiv:2010.05915] [INSPIRE].

[15] L. Darmé, B. Fuks and F. Maltoni, *Top-philic heavy resonances in four-top final states and their EFT interpretation*, *JHEP* **09** (2021) 143 [arXiv:2104.09512] [INSPIRE].

[16] Y. Chung and F. Goertz, *Third-generation-philic hidden naturalness*, *Phys. Rev. D* **110** (2024) 115019 [arXiv:2311.17169] [INSPIRE].

[17] D. Choudhury, K. Deka and L.K. Saini, *Boosted four-top production at the LHC: A window to Randall-Sundrum or extended color symmetry*, *Phys. Rev. D* **110** (2024) 075020 [arXiv:2404.04409] [INSPIRE].

[18] J. de Blas, M. Chala and J. Santiago, *Renormalization Group Constraints on New Top Interactions from Electroweak Precision Data*, *JHEP* **09** (2015) 189 [arXiv:1507.00757] [INSPIRE].

[19] S. Dawson and P.P. Giardino, *Electroweak and QCD corrections to Z and W pole observables in the standard model EFT*, *Phys. Rev. D* **101** (2020) 013001 [arXiv:1909.02000] [INSPIRE].

[20] U. Haisch and L. Schnell, *Precision tests of third-generation four-quark operators: one- and two-loop matching*, *JHEP* **02** (2025) 038 [arXiv:2410.13304] [INSPIRE].

[21] L. Alasfar, J. de Blas and R. Gröber, *Higgs probes of top quark contact interactions and their interplay with the Higgs self-coupling*, *JHEP* **05** (2022) 111 [arXiv:2202.02333] [INSPIRE].

JHEP01(2026)025

[22] S. Di Noi et al., *$\gamma 5$ schemes and the interplay of SMEFT operators in the Higgs-gluon coupling*, *Phys. Rev. D* **109** (2024) 095024 [arXiv:2310.18221] [INSPIRE].

[23] C. Degrande et al., *Automated one-loop computations in the standard model effective field theory*, *Phys. Rev. D* **103** (2021) 096024 [arXiv:2008.11743] [INSPIRE].

[24] C. Degrande, R. Rosenfeld and A. Vasquez, *Collider sensitivity to SMEFT heavy-quark operators at one-loop in top-quark processes*, *JHEP* **07** (2024) 114 [arXiv:2402.06528] [INSPIRE].

[25] L. Silvestrini and M. Valli, *Model-independent Bounds on the Standard Model Effective Theory from Flavour Physics*, *Phys. Lett. B* **799** (2019) 135062 [arXiv:1812.10913] [INSPIRE].

[26] M.S. Chanowitz, M. Furman and I. Hinchliffe, *The Axial Current in Dimensional Regularization*, *Nucl. Phys. B* **159** (1979) 225 [INSPIRE].

[27] G. 't Hooft and M.J.G. Veltman, *Regularization and Renormalization of Gauge Fields*, *Nucl. Phys. B* **44** (1972) 189 [INSPIRE].

[28] P. Breitenlohner and D. Maison, *Dimensional Renormalization and the Action Principle*, *Commun. Math. Phys.* **52** (1977) 11 [INSPIRE].

[29] S. Di Noi, R. Gröber and P. Olgoso, *Mapping between γ_5 schemes in the Standard Model Effective Field Theory*, *JHEP* **09** (2025) 027 [arXiv:2504.00112] [INSPIRE].

[30] G. Heinrich and J. Lang, *Combining chromomagnetic and four-fermion operators with leading SMEFT operators for $gg \to hh$ at NLO QCD*, *JHEP* **05** (2024) 121 [arXiv:2311.15004] [INSPIRE].

[31] A.J. Buras, M. Jamin, M.E. Lautenbacher and P.H. Weisz, *Effective Hamiltonians for $\Delta S = 1$ and $\Delta B = 1$ nonleptonic decays beyond the leading logarithmic approximation*, *Nucl. Phys. B* **370** (1992) 69 [*Addendum ibid.* **375** (1992) 501] [INSPIRE].

[32] A.J. Buras, M. Jamin, M.E. Lautenbacher and P.H. Weisz, *Two loop anomalous dimension matrix for $\Delta S = 1$ weak nonleptonic decays I: $\mathcal{O}(\alpha_s^2)$*, *Nucl. Phys. B* **400** (1993) 37 [hep-ph/9211304] [INSPIRE].

[33] M. Ciuchini et al., *Scheme independence of the effective Hamiltonian for $b \to s\gamma$ and $b \to sg$ decays*, *Phys. Lett. B* **316** (1993) 127 [hep-ph/9307364] [INSPIRE].

[34] K. Adel and Y.-P. Yao, *$O(\alpha_s)$ calculation of the decays $b \to s + \gamma$ and $b \to s + g$*, *Phys. Rev. D* **49** (1994) 4945 [hep-ph/9308349] [INSPIRE].

[35] M. Ciuchini, E. Franco, L. Reina and L. Silvestrini, *Leading order QCD corrections to $b \to s\gamma$ and $b \to sg$ decays in three regularization schemes*, *Nucl. Phys. B* **421** (1994) 41 [hep-ph/9311357] [INSPIRE].

[36] T. Corbett, A. Martin and M. Trott, *Consistent higher order $\sigma(\mathcal{GG} \to h)$, $\Gamma(h \to \mathcal{GG})$ and $\Gamma(h \to \gamma\gamma)$ in geoSMEFT*, *JHEP* **12** (2021) 147 [arXiv:2107.07470] [INSPIRE].

[37] A. Martin and M. Trott, *More accurate $\sigma\left(\mathcal{GG} \to h\right), \Gamma\left(h \to \mathcal{GG}, \mathcal{AA}, \overline{\Psi}\Psi\right)$ and Higgs width results via the geoSMEFT*, *JHEP* **01** (2024) 170 [arXiv:2305.05879] [INSPIRE].

[38] A. Biekötter, B.D. Pecjak, D.J. Scott and T. Smith, *Electroweak input schemes and universal corrections in SMEFT*, *JHEP* **07** (2023) 115 [arXiv:2305.03763] [INSPIRE].

[39] B. Grzadkowski, M. Iskrzynski, M. Misiak and J. Rosiek, *Dimension-Six Terms in the Standard Model Lagrangian*, *JHEP* **10** (2010) 085 [arXiv:1008.4884] [INSPIRE].

[40] D. Barducci et al., *Interpreting top-quark LHC measurements in the standard-model effective field theory*, arXiv:1802.07237 [INSPIRE].

JHEP01(2026)025

[41] J. Alwall et al., *The automated computation of tree-level and next-to-leading order differential cross sections, and their matching to parton shower simulations*, *JHEP* **07** (2014) 079 [arXiv:1405.0301] [INSPIRE].

[42] NNPDF collaboration, *Parton distributions from high-precision collider data*, *Eur. Phys. J. C* **77** (2017) 663 [arXiv:1706.00428] [INSPIRE].

[43] A. Buckley et al., *LHAPDF6: parton density access in the LHC precision era*, *Eur. Phys. J. C* **75** (2015) 132 [arXiv:1412.7420] [INSPIRE].

[44] A. Denner, S. Dittmaier, M. Roth and D. Wackeroth, *Electroweak radiative corrections to $e^+e^- \to WW \to 4$ fermions in double pole approximation: The RACOONWW approach*, *Nucl. Phys. B* **587** (2000) 67 [hep-ph/0006307] [INSPIRE].

[45] S. Dittmaier and M. Krämer, *Electroweak radiative corrections to W boson production at hadron colliders*, *Phys. Rev. D* **65** (2002) 073007 [hep-ph/0109062] [INSPIRE].

[46] I. Brivio et al., *Electroweak input parameters*, arXiv:2111.12515 [INSPIRE].

[47] J.G. Korner, D. Kreimer and K. Schilcher, *A Practicable γ_5 scheme in dimensional regularization*, *Z. Phys. C* **54** (1992) 503 [INSPIRE].

[48] R. Aoude et al., *Renormalisation group effects on SMEFT interpretations of LHC data*, *JHEP* **09** (2023) 191 [arXiv:2212.05067] [INSPIRE].

[49] F. Maltoni, G. Ventura and E. Vryonidou, *Impact of SMEFT renormalisation group running on Higgs production at the LHC*, *JHEP* **12** (2024) 183 [arXiv:2406.06670] [INSPIRE].

[50] S. Di Noi and R. Gröber, *Renormalisation group running effects in $pp \to t\bar{t}h$ in the Standard Model Effective Field Theory*, *Eur. Phys. J. C* **84** (2024) 403 [arXiv:2312.11327] [INSPIRE].

[51] S. Di Noi, R. Gröber and M.K. Mandal, *Two-loop running effects in Higgs physics in Standard Model Effective Field Theory*, *JHEP* **12** (2025) 220 [arXiv:2408.03252] [INSPIRE].

[52] R. Aoude, H. El Faham, F. Maltoni and E. Vryonidou, *Complete SMEFT predictions for four top quark production at hadron colliders*, *JHEP* **10** (2022) 163 [arXiv:2208.04962] [INSPIRE].

[53] R. Frederix, D. Pagani and M. Zaro, *Large NLO corrections in $t\bar{t}W^{\pm}$ and $t\bar{t}t\bar{t}$ hadroproduction from supposedly subleading EW contributions*, *JHEP* **02** (2018) 031 [arXiv:1711.02116] [INSPIRE].

[54] I. Brivio et al., *O new physics, where art thou? A global search in the top sector*, *JHEP* **02** (2020) 131 [arXiv:1910.03606] [INSPIRE].

[55] D. Kreimer, *The role of gamma(5) in dimensional regularization*, hep-ph/9401354 [INSPIRE].

[56] L. Chen, *An observation on Feynman diagrams with axial anomalous subgraphs in dimensional regularization with an anticommuting γ_5*, *JHEP* **11** (2023) 030 [arXiv:2304.13814] [INSPIRE].

[57] L. Chen, *A procedure g5anchor to anchor γ_5 in Feynman diagrams for the Standard Model*, *JHEP* **05** (2025) 109 [arXiv:2409.08099] [INSPIRE].

[58] H. Bélusca-Maïto, A. Ilakovac, M. Mađor-Božinović and D. Stöckinger, *Dimensional regularization and Breitenlohner-Maison/'t Hooft-Veltman scheme for γ_5 applied to chiral YM theories: full one-loop counterterm and RGE structure*, *JHEP* **08** (2020) 024 [arXiv:2004.14398] [INSPIRE].

[59] H. Bélusca-Maïto et al., *Two-loop application of the Breitenlohner-Maison/'t Hooft-Veltman scheme with non-anticommuting γ_5: full renormalization and symmetry-restoring counterterms in an abelian chiral gauge theory*, *JHEP* **11** (2021) 159 [arXiv:2109.11042] [INSPIRE].

JHEP01(2026)025

[60] C. Cornella, F. Feruglio and L. Vecchi, *Gauge invariance and finite counterterms in chiral gauge theories*, *JHEP* **02** (2023) 244 [arXiv:2205.10381] [INSPIRE].

[61] H. Bélusca-Maïto et al., *Introduction to Renormalization Theory and Chiral Gauge Theories in Dimensional Regularization with Non-Anticommuting γ_5*, *Symmetry* **15** (2023) 622 [arXiv:2303.09120] [INSPIRE].

[62] P. Olgoso Ruiz and L. Vecchi, *Spurious gauge-invariance and γ_5 in dimensional regularization*, *JHEP* **12** (2024) 080 [arXiv:2406.17013] [INSPIRE].

[63] A. von Manteuffel, D. Stöckinger and M. Weißwange, *Four-loop renormalisation of chiral gauge theories with non-anticommuting γ_5 in the BMHV scheme*, *JHEP* **08** (2025) 088 [arXiv:2506.12253] [INSPIRE].

[64] P.L. Ebert, P. Kühler, D. Stöckinger and M. Weißwange, *Shedding light on evanescent shadows — Exploration of non-anticommuting γ_5 in Dimensional Regularisation*, *JHEP* **01** (2025) 114 [arXiv:2411.02543] [INSPIRE].

[65] C. Arzt, M.B. Einhorn and J. Wudka, *Patterns of deviation from the standard model*, *Nucl. Phys. B* **433** (1995) 41 [hep-ph/9405214] [INSPIRE].

[66] G. Buchalla, G. Heinrich, C. Müller-Salditt and F. Pandler, *Loop counting matters in SMEFT*, *SciPost Phys.* **15** (2023) 088 [arXiv:2204.11808] [INSPIRE].

[67] CMS collaboration, *A portrait of the Higgs boson by the CMS experiment ten years after the discovery*, *Nature* **607** (2022) 60 [arXiv:2207.00043] [INSPIRE].

[68] LHC Higgs Cross Section Working Group collaboration, *Handbook of LHC Higgs Cross Sections: 4. Deciphering the Nature of the Higgs Sector*, *CERN Yellow Rep. Monogr.* **2** (2017) 1 [arXiv:1610.07922] [INSPIRE].

[69] T. Inami, T. Kubota and Y. Okada, *Effective Gauge Theory and the Effect of Heavy Quarks in Higgs Boson Decays*, *Z. Phys. C* **18** (1983) 69 [INSPIRE].

[70] A. Djouadi, M. Spira and P.M. Zerwas, *Production of Higgs bosons in proton colliders: QCD corrections*, *Phys. Lett. B* **264** (1991) 440 [INSPIRE].

[71] M. Spira, A. Djouadi, D. Graudenz and P.M. Zerwas, *Higgs boson production at the LHC*, *Nucl. Phys. B* **453** (1995) 17 [hep-ph/9504378] [INSPIRE].

[72] K.G. Chetyrkin, B.A. Kniehl and M. Steinhauser, *Hadronic Higgs decay to order α_s^4*, *Phys. Rev. Lett.* **79** (1997) 353 [hep-ph/9705240] [INSPIRE].

[73] P.A. Baikov and K.G. Chetyrkin, *Top Quark Mediated Higgs Boson Decay into Hadrons to Order α_s^5*, *Phys. Rev. Lett.* **97** (2006) 061803 [hep-ph/0604194] [INSPIRE].

[74] S. Actis, G. Passarino, C. Sturm and S. Uccirati, *NNLO Computational Techniques: The Cases $H \to \gamma\gamma$ and $H \to gg$*, *Nucl. Phys. B* **811** (2009) 182 [arXiv:0809.3667] [INSPIRE].

[75] S. Actis, G. Passarino, C. Sturm and S. Uccirati, *NLO Electroweak Corrections to Higgs Boson Production at Hadron Colliders*, *Phys. Lett. B* **670** (2008) 12 [arXiv:0809.1301] [INSPIRE].

[76] H.Q. Zheng and D.D. Wu, *First order QCD corrections to the decay of the Higgs boson into two photons*, *Phys. Rev. D* **42** (1990) 3760 [INSPIRE].

[77] A. Djouadi, M. Spira, J.J. van der Bij and P.M. Zerwas, *QCD corrections to gamma gamma decays of Higgs particles in the intermediate mass range*, *Phys. Lett. B* **257** (1991) 187 [INSPIRE].

[78] S. Dawson and R.P. Kauffman, *QCD corrections to $H \to \gamma\gamma$*, *Phys. Rev. D* **47** (1993) 1264 [INSPIRE].

JHEP01(2026)025

[79] A. Djouadi, M. Spira and P.M. Zerwas, *Two photon decay widths of Higgs particles*, *Phys. Lett. B* **311** (1993) 255 [hep-ph/9305335] [INSPIRE].

[80] K. Melnikov and O.I. Yakovlev, *Higgs —> two photon decay: QCD radiative correction*, *Phys. Lett. B* **312** (1993) 179 [hep-ph/9302281] [INSPIRE].

[81] M. Inoue, R. Najima, T. Oka and J. Saito, *QCD corrections to two photon decay of the Higgs boson and its reverse process*, *Mod. Phys. Lett. A* **9** (1994) 1189 [INSPIRE].

[82] A. Djouadi, J. Kalinowski and M. Spira, *HDECAY: A Program for Higgs boson decays in the standard model and its supersymmetric extension*, *Comput. Phys. Commun.* **108** (1998) 56 [hep-ph/9704448] [INSPIRE].

[83] ALEPH et al. collaborations, *Precision electroweak measurements on the Z resonance*, *Phys. Rept.* **427** (2006) 257 [hep-ex/0509008] [INSPIRE].

[84] CMS collaboration, *Measurement of differential $t\bar{t}$ production cross sections in the full kinematic range using lepton+jets events from proton-proton collisions at $\sqrt{s} = 13$ TeV*, *Phys. Rev. D* **104** (2021) 092013 [arXiv:2108.02803] [INSPIRE].

[85] ATLAS collaboration, *Measurements of top-quark pair differential and double-differential cross-sections in the ℓ+jets channel with pp collisions at $\sqrt{s} = 13$ TeV using the ATLAS detector*, *Eur. Phys. J. C* **79** (2019) 1028 [*Erratum ibid.* **80** (2020) 1092] [arXiv:1908.07305] [INSPIRE].

[86] ATLAS collaboration, *Measurement of the associated production of a top-antitop-quark pair and a Higgs boson decaying into a $b\bar{b}$ pair in pp collisions at $\sqrt{s} = 13$ TeV using the ATLAS detector at the LHC*, *Eur. Phys. J. C* **85** (2025) 210 [arXiv:2407.10904] [INSPIRE].

[87] ATLAS collaboration, *A detailed map of Higgs boson interactions by the ATLAS experiment ten years after the discovery*, *Nature* **607** (2022) 52 [*Erratum ibid.* **612** (2022) E24] [arXiv:2207.00092] [INSPIRE].

[88] M. van Beekveld, A. Kulesza and L.M. Valero, *Threshold Resummation for the Production of Four Top Quarks at the LHC*, *Phys. Rev. Lett.* **131** (2023) 211901 [arXiv:2212.03259] [INSPIRE].

[89] ATLAS collaboration, *Measurements of inclusive and differential fiducial cross-sections of $t\bar{t}$ production with additional heavy-flavour jets in proton-proton collisions at $\sqrt{s} = 13$ TeV with the ATLAS detector*, *JHEP* **04** (2019) 046 [arXiv:1811.12113] [INSPIRE].

[90] CMS collaboration, *Measurement of the cross section for $t\bar{t}$ production with additional jets and b jets in pp collisions at $\sqrt{s} = 13$ TeV*, *JHEP* **07** (2020) 125 [arXiv:2003.06467] [INSPIRE].

[91] I. Brivio and M. Trott, *Scheming in the SMEFT... and a reparameterization invariance!*, *JHEP* **07** (2017) 148 [*Addendum ibid.* **05** (2018) 136] [arXiv:1701.06424] [INSPIRE].

[92] S. Frixione, P. Nason and G. Ridolfi, *A Positive-weight next-to-leading-order Monte Carlo for heavy flavour hadroproduction*, *JHEP* **09** (2007) 126 [arXiv:0707.3088] [INSPIRE].

[93] P. Nason, *A new method for combining NLO QCD with shower Monte Carlo algorithms*, *JHEP* **11** (2004) 040 [hep-ph/0409146] [INSPIRE].

[94] S. Frixione, P. Nason and C. Oleari, *Matching NLO QCD computations with Parton Shower simulations: the POWHEG method*, *JHEP* **11** (2007) 070 [arXiv:0709.2092] [INSPIRE].

[95] S. Alioli, P. Nason, C. Oleari and E. Re, *A general framework for implementing NLO calculations in shower Monte Carlo programs: the POWHEG BOX*, *JHEP* **06** (2010) 043 [arXiv:1002.2581] [INSPIRE].

JHEP01(2026)025

[96] T. Sjostrand, S. Mrenna and P.Z. Skands, *A Brief Introduction to PYTHIA 8.1*, *Comput. Phys. Commun.* **178** (2008) 852 [arXiv:0710.3820] [INSPIRE].

[97] M. Czakon and A. Mitov, *Top++: A program for the Calculation of the Top-Pair Cross-Section at Hadron Colliders*, *Comput. Phys. Commun.* **185** (2014) 2930 [arXiv:1112.5675] [INSPIRE].

[98] M. Beneke, P. Falgari, S. Klein and C. Schwinn, *Hadronic top-quark pair production with NNLL threshold resummation*, *Nucl. Phys. B* **855** (2012) 695 [arXiv:1109.1536] [INSPIRE].

[99] M. Cacciari et al., *Top-pair production at hadron colliders with next-to-next-to-leading logarithmic soft-gluon resummation*, *Phys. Lett. B* **710** (2012) 612 [arXiv:1111.5869] [INSPIRE].

[100] P. Bärnreuther, M. Czakon and A. Mitov, *Percent Level Precision Physics at the Tevatron: First Genuine NNLO QCD Corrections to $q\bar{q} \to t\bar{t} + X$*, *Phys. Rev. Lett.* **109** (2012) 132001 [arXiv:1204.5201] [INSPIRE].

[101] M. Czakon and A. Mitov, *NNLO corrections to top-pair production at hadron colliders: the all-fermionic scattering channels*, *JHEP* **12** (2012) 054 [arXiv:1207.0236] [INSPIRE].

[102] M. Czakon and A. Mitov, *NNLO corrections to top pair production at hadron colliders: the quark-gluon reaction*, *JHEP* **01** (2013) 080 [arXiv:1210.6832] [INSPIRE].

[103] M. Czakon, P. Fiedler and A. Mitov, *Total Top-Quark Pair-Production Cross Section at Hadron Colliders Through $O(\alpha_S^4)$*, *Phys. Rev. Lett.* **110** (2013) 252004 [arXiv:1303.6254] [INSPIRE].

[104] J.M. Lindert, K. Kudashkin, K. Melnikov and C. Wever, *Higgs bosons with large transverse momentum at the LHC*, *Phys. Lett. B* **782** (2018) 210 [arXiv:1801.08226] [INSPIRE].

[105] HDECAY collaboration, *HDECAY: Twenty$_{++}$ years after*, *Comput. Phys. Commun.* **238** (2019) 214 [arXiv:1801.09506] [INSPIRE].

[106] M. Bonetti, K. Melnikov and L. Tancredi, *Higher order corrections to mixed QCD-EW contributions to Higgs boson production in gluon fusion*, *Phys. Rev. D* **97** (2018) 056017 [*Erratum ibid.* **97** (2018) 099906] [arXiv:1801.10403] [INSPIRE].

[107] F. Dulat, A. Lazopoulos and B. Mistlberger, *iHixs 2 — Inclusive Higgs cross sections*, *Comput. Phys. Commun.* **233** (2018) 243 [arXiv:1802.00827] [INSPIRE].

[108] R.V. Harlander, J. Klappert, S. Liebler and L. Simon, *vh@nnlo-v2: New physics in Higgs Strahlung*, *JHEP* **05** (2018) 089 [arXiv:1802.04817] [INSPIRE].

[109] M. Cacciari et al., *Fully Differential Vector-Boson-Fusion Higgs Production at Next-to-Next-to-Leading Order*, *Phys. Rev. Lett.* **115** (2015) 082002 [*Erratum ibid.* **120** (2018) 139901] [arXiv:1506.02660] [INSPIRE].

[110] A. Falkowski et al., *Rosetta: an operator basis translator for Standard Model effective field theory*, *Eur. Phys. J. C* **75** (2015) 583 [arXiv:1508.05895] [INSPIRE].

[111] A. Falkowski, *Higgs Basis: Proposal for an EFT basis choice for LHC HXSWG*, LHCHXSWG-INT-2015-001 (2015).

[112] M. Thomas Arun, K. Deka and T. Srivastava, *Constraining SMEFT BSM scenarios with EWPO and Δ_{CKM}*, *Pramana* **99** (2025) 145 [arXiv:2301.09273] [INSPIRE].

JHEP01(2026)025